Prohibitin depletion suppresses mitochondrial, lipogenic and autophagic defects of SGK-1 mutant extending lifespan; implication of autophagy and the UPR^{mt}.

Blanca Hernando-Rodríguez[1,2,*], Mercedes M. Pérez-Jiménez[1,2,*], María Jesús Rodríguez-Palero[1,2], Antoni Pla[1,2], Manuel David Martínez-Bueno[1,2], Patricia de la Cruz Ruiz[1,2], Roxani Gatsi[1,2] and Marta Artal-Sanz[1,2 #]

[1]Andalusian Centre for Developmental Biology, Consejo Superior de Investigaciones Científicas/Junta de Andalucía/Universidad Pablo de Olavide, Seville, Spain

[2]Department of Molecular Biology and Biochemical Engineering, Universidad Pablo de Olavide, Seville, Spain

[#]Correspondence to: martsan@upo.es

*Equal contribution

Aging is a complex and multifactorial process influenced by different pathways interacting in a not completely defined manner. Mitochondrial prohibitins (PHBs) are strongly evolutionarily conserved proteins with a peculiar effect on lifespan. While their depletion shortens lifespan of wild type animals, it enhances longevity of a plethora of metabolically compromised mutants, including target of rapamycin complex 2 (TORC2) mutants *sgk-1* and *rict-1*. Intriguingly, TORC2 mutants induce the mitochondrial unfolded protein response (UPR^{mt}), while reducing the strong UPR^{mt} elicited by PHB depletion. To understand this inverse correlation between lifespan and activation of the UPR^{mt}, we studied the interaction of TORC2 signaling with mitochondrial quality control mechanisms including mitophagy, the UPR^{mt} and autophagy. Our data revealed that *sgk-1* mutants have increased mitochondrial size, respiration rate and ROS production, phenotypes suppressed by PHB depletion. A transcription factor RNAi screen identified lipid and sterol homeostasis as UPR^{mt} modulators in *sgk-1* mutants. In accordance, *sgk-1(ok538)* show impaired lipogenesis, yolk formation and autophagy flux, plausibly due to altered organelle contacts. Remarkably, all these features are suppressed by PHB depletion. Lifespan analysis showed that autophagy and the UPR^{mt}, but not mitophagy, are required for the enhanced longevity caused by PHB depletion in *sgk-1* mutants. Because the UPR^{mt} transcription factor ATFS-1 activates autophagy, we hypothesize that UPR^{mt} induction upon PHB depletion extends lifespan of *sgk-1* mutants through autophagy. Our results strongly suggest that PHB depletion suppresses the autophagy defects of *sgk-1* mutants by altering membrane lipid composition at ER-mitochondria contact sites, where TORC2 localizes.

42 ## Introduction

43 Mitochondrial function, nutrient signalling and autophagy regulate aging across phyla.
44 However, the exact mechanisms and how they interact to modulate lifespan remain still
45 elusive. The mitochondrial prohibitin (PHB) complex is a strongly evolutionarily
46 conserved ring-like macromolecular structure [1, 2]. While deletion of PHB does not
47 cause any observable growth phenotype in the unicellular yeast *Saccharomyces*
48 *cerevisiae* [3], in *Caenorhabditis elegans* the PHB complex is required for embryonic
49 development and its postembryonic depletion leads to morphological abnormalities in
50 the somatic gonad and sterility [4]. Prohibitins have been implicated in several age-
51 related diseases [5, 6] and are involved in mitochondrial morphogenesis and
52 maintenance of mitochondrial membranes by acting as chaperones [7] and scaffolds [8].
53 Recently, PHB-2 has been described essential for Parkin mediated mitophagy [9].

54 PHB depletion perturbs mitochondrial homeostasis causing an induction of the
55 mitochondrial unfolded protein response, UPR^{mt} [10-12], and has an opposing effect on
56 lifespan depending on the genetic background. Loss of PHB by RNAi shortens lifespan
57 in wild type worms, whereas it increases lifespan in different metabolically compromised
58 backgrounds such as mutants of the Insulin/IGF-1 signalling (IIS) pathway or mutants
59 with compromised mitochondrial function or fat metabolism [13]. In particular, PHB
60 depletion increases lifespan of the already long-lived *daf-2(e1370)* mutants, where the
61 induction of the UPR^{mt} is reduced [14]. Through analysing known kinases acting
62 downstream of the insulin receptor DAF-2 [15], we found that loss of function of SGK-1
63 recapitulates the enhanced longevity and the reduced UPR^{mt} activation observed upon
64 PHB depletion in *daf-2* mutants [14]. SGK-1 belongs to the AGC kinase family and is the
65 sole *C. elegans* homologue of the mammalian Serum- and Glucocorticoid-inducible
66 Kinase. Its expression is induced upon diverse stimuli, including overload of calcium [16],

67 heat shock, oxidative or osmotic stress [17-19], besides of glucocorticoids, cytokines and
68 growth factors [20, 21]. Its activation is dependent on PI3K and has been involved in
69 response to oxidative stress and DNA damage, among others [22]. In addition of acting
70 in the IIS pathway, SGK-1 regulates aging and mitochondrial homeostasis through a
71 parallel pathway, as part of TORC2 (Target Of Rapamycin Complex 2), downstream of
72 RICT-1. Interestingly, *daf-2;sgk-1* double mutants show a further lifespan increment and
73 a further reduction of the UPR^{mt} upon PHB depletion [14].

74 Work in yeast has demonstrated that Ypk1, the yeast homologue of SGK-1, is the
75 relevant target of TORC2 involved in sphingolipid synthesis and ceramide signalling
76 having an essential role in lipid membrane homeostasis and affecting cell size and
77 growth rate [23-25]. Interestingly, TORC2-Ypk1 controls sphingolipid homeostasis by
78 sensing and regulating ROS [26]. Moreover, TORC2-Ypk1 regulates autophagy upon
79 amino acid starvation [27] and modulates the autophagy flux by controlling mitochondrial
80 respiration and calcium signalling [28, 29], although the molecular mechanism remains
81 unknown. In worms, SGK-1 regulates development, fat metabolism, stress responses
82 and lifespan in a complex and controversial manner, partially explained by the different
83 alleles under study and the different growing conditions [14, 15, 30-36].

84 To better understand how SGK-1 regulates lifespan and mitochondrial function, we
85 explored the interaction between PHB and SGK-1. Our results show that long-lived *sgk-*
86 *1(ok538)* mutants have altered mitochondrial structure and function, phenotypes that are
87 suppressed by PHB depletion. We further examined the interaction of SGK-1 with
88 mitochondrial quality control mechanisms, the UPR^{mt} and mitophagy, both activated in
89 *sgk-1* and *phb-1* deficient animals. While SGK-1 protein levels increased upon inhibition
90 of the UPR^{mt} and mitophagy in otherwise wild type animals, in the absence of the PHB
91 complex, SGK-1 expression levels increased upon inhibition of the UPR^{mt}, but not
92 mitophagy. A transcription factor RNAi screen identified membrane lipid homeostasis as

93 a mechanism implicated in the maintenance of mitochondrial function by SGK-1. In
94 agreement with that, electron microscopy analysis showed defects in organelle
95 membrane contact sites in *sgk-1* mutants, leading to defective lipogenesis and
96 lipoprotein production and a blockage of the autophagic flux. Remarkably, these
97 phenotypes are suppressed by PHB depletion. Further, lifespan analyses showed that
98 autophagy and the UPR^{mt} are required for the enhanced longevity of *sgk-1* mutants upon
99 PHB depletion, while mitophagy is not. Surprisingly, inhibition of mitophagy extends the
100 lifespan of *sgk-1* mutants and PHB deficient worms. We discuss our observations in light
101 of the conserved role of TORC2 in lipid membrane biology and the proposed role of the
102 PHB complex and TORC2 at mitochondria-associated endoplasmic reticulum (ER)
103 membranes (MAM).

104 Results

105 *sgk-1* mutants have altered mitochondrial structure and function, which are 106 suppressed by prohibitin depletion

107 In *C. elegans*, loss of function of SGK-1 causes a delay in development [33] as well as
108 reduced brood and body size [31]. These phenotypes are consistent with phenotypes
109 observed in mitochondrial mutants [37] and mitochondrial fragmentation has been
110 reported upon *sgk-1* depletion in muscle [38] and intestine [35]. In addition, worms
111 lacking the TORC2 component RICT-1 or the downstream kinase SGK-1, have an
112 induced mitochondrial unfolded protein response (UPR^{mt}) [14]. Here, we analyzed
113 whether mitophagy, another mitochondrial quality control mechanism, might be activated
114 in *sgk-1* deletion mutants. For this purpose, we used a mitophagy reporter based on
115 PINK-1 protein [39], a serine threonine protein kinase that, when mitochondria are
116 depolarized, accumulates in the outer mitochondrial membrane and targets mitochondria
117 for selective autophagy [40, 41]. We observed that depletion of *sgk-1* increased PINK-1

118 protein levels (Figure 1A). Additionally, we show that inducing mitochondrial stress via
119 depletion of *phb-1* or *atfs-1,* the key UPR^{mt} regulator, had similar effects, increasing
120 PINK-1 protein levels (Figure 1A). This observation further suggests that *sgk*-1 mutants
121 suffer from mitochondrial stress.

122 To better define the mitochondrial defect of *sgk-1* deletion mutants we performed
123 transmission electron microscopy (TEM) analysis. We observed swollen and bigger
124 mitochondria in *sgk-1* mutants as compared to wild type worms in all tissues analyzed
125 (hypodermis, muscle and intestine) at both, day one and day five of adulthood (Figure
126 1B and Figure S1, respectively). No obvious mitochondrial fragmentation or severe
127 cristae defects in the intestine could be observed in the TEM sections analyzed, as
128 previously described [35].

129 While shortening lifespan of otherwise wild type animals, PHB depletion extends lifespan
130 of TORC2 mutants, *rict-1* and *sgk-1*, as it does with other mitochondrial mutants [13, 14].
131 To better understand this interaction, we measured mitochondrial performance in *sgk-1*
132 mutants in the presence and absence of the PHB complex, during aging (Figures 1C-F
133 and Figure S2). Mitochondrial respiration is recognized as an indicator of mitochondrial
134 health and its measurement at the level of oxidative phosphorylation has emerged as a
135 proxy for mitochondrial dysfunction [42]. At the young adult stage, *sgk-1* mutants showed
136 a dramatic increase in basal oxygen consumption rate (OCR) compared to wild type
137 worms (Figures 1C and 1D), consistent with the previous finding that mammalian
138 mTORC2/rictor knockdown leads to an increase in mitochondrial respiration in
139 mammalian cells [43]. The increased respiration rate of *sgk-1* mutants was suppressed
140 by PHB depletion. Lack of PHB also reduced the OCR of wild type worms (Figures 1C
141 and 1D). At day 6 of adulthood, the OCR was generally reduced (Supplementary figure
142 S2b) as already described [44], except for *phb-1(RNAi)* worms. While wild type and *sgk-*
143 *1* mutants had a similar respiration rate, PHB depletion increased the OCR in both

144 backgrounds (Figure S2A and S2B). This suggests that mitochondrial function declines
145 with age in wild type animals but this decline occurs at a higher rate in *sgk-1* mutants,
146 whereas in PHB depleted worms, where already at the young adult stage respiration is
147 compromised, it remains relatively constant.

148 In concordance with a higher basal respiration, at the young adult stage *sgk-1* mutants
149 had a higher maximal respiratory capacity compared to wild type worms, which was fully
150 suppressed by PHB depletion. PHB depletion also reduced the maximal respiratory
151 capacity of wild type worms (Figure 1D). The spare capacity or reserve capacity is the
152 difference between maximal and basal OCR and it is defined as the amount of oxygen
153 that is available for cells under stress or increased energy demands. *sgk-1* mutants
154 showed reduced spare respiratory capacity, as the difference between maximal and
155 basal OCR was diminished compared to wild type animals. Additionally, depletion of *phb-*
156 *1* reduced the spare capacity in both backgrounds (Figure 1D). By calculating the oxygen
157 consumption linked to ATP production, derived from inhibiting ATP synthase with
158 oligomycin, we observed an increased ATP-linked OCR in *sgk-1* mutants (Figure 1E),
159 which may correspond to a higher energy demand. Differently, *phb-1(RNAi)* reduced the
160 ATP-linked OCR (Figure 1E) both in otherwise wild type worms as well as in *sgk-1*
161 mutants, suggesting a severe damage in the oxidative phosphorylation system. Again,
162 depletion of the PHB complex reversed *sgk-1* mutants' phenotypes, bringing ATP-linked
163 OCR to wild-type levels (Figure 1E). The O_2 consumed after sodium azide (NaN_3)
164 injection corresponds to the respiration caused by other cellular processes than oxidative
165 phosphorylation, such as non-mitochondrial NADPH oxidases or reactive oxygen
166 species production. Interestingly, *sgk-1* mutants showed an increased non-mitochondrial
167 respiration compared to wild type at the young adult stage, which was suppressed by
168 PHB depletion. Lack of PHB also reduced non-mitochondrial respiration in wild type
169 worms (Figure 1F).

170 Mitochondrial respiration is the most relevant source of cellular ROS. We thus evaluated
171 ROS levels in *sgk-1* mutants in the presence and absence of the PHB complex. We
172 measured ROS formation at the young adult stage using the dye H2-DCFDA (Figure
173 1G). In agreement with the observed increment in both, mitochondrial and non-
174 mitochondrial respiration, *sgk-1* mutants showed dramatically elevated ROS levels in
175 comparison to wild type worms, as previously published in other organisms [26, 45].
176 Depletion of *phb-1* increased ROS levels in wild type worms (Figure 1G and [13]).
177 However, depletion of *phb-1* reduced ROS levels in *sgk-1* mutants (Figure 1G). Since
178 H2-DCFDA measures mostly cytosolic ROS, these results indicate that *sgk-1* mutants
179 have high levels of cytosolic ROS that are reduced upon *phb-1* depletion. Nevertheless,
180 even if we were not able to measure mitochondrial ROS levels, PHB depletion has been
181 shown to increase mitochondrial basal ROS production [46] and the increment of
182 mitochondrial ROS extends lifespan of mitochondrial mutants with high levels of
183 cytoplasmic ROS [47]. We then wondered whether the enhancement of lifespan upon
184 *phb-1* depletion in *sgk-1* mutants may be due to an increment of specifically
185 mitochondrial ROS levels. Lack of the cytosolic enzyme, *sod-1*, did not affect lifespan of
186 wild type worms, while lack of the mitochondrial superoxide dismutase, *sod-2*, increased
187 wild type lifespan (Figure S2C, Table S1 and [48, 49]). Interestingly, lack of *sod-1*
188 reduced lifespan of *sgk-1* mutants, indicating that increased cytosolic ROS is detrimental
189 for *sgk-1* lifespan, while depletion of *sod-2*, increased lifespan of *sgk-1* mutants (Figure
190 S2D, Table S1), similar to mitochondrial mutants [47]. In order to test if mitochondrial
191 ROS generation upon PHB depletion extends lifespan of *sgk-1* mutants, we treated
192 animals with the antioxidant N-acetyl-cysteine (NAC). NAC did not affect the lifespan of
193 wild type worms or *sgk-1* mutants, while it shortened that of *phb-1* depleted animals,
194 both in wild type and in *sgk-1* mutant backgrounds (Figure S2E and S2F, Table S1).
195 Therefore, we cannot conclude that ROS is responsible for the lifespan extension
196 conferred by PHB depletion to *sgk-1* mutants.

197 Finally, we wondered whether depletion of the PHB complex would suppress the
198 increased mitochondrial size observed in *sgk-1* mutants. TEM analysis of muscle
199 mitochondria showed that *phb-1* depletion drastically reduced mitochondrial size in *sgk-*
200 *1* mutants, and resulted in mitochondrial fragmentation as it happens in otherwise wild
201 type worms [4] (Figure 1H and Figure S3).

202 **SGK-1 protein levels differentially respond to mitochondrial quality control**
203 **mechanisms, UPR^{mt} and mitophagy, upon PHB depletion.**

204 Our results suggest that TORC2/SGK-1 regulates mitochondrial performance as *sgk-1*
205 loss of function mutants have altered mitochondrial size and respiration, induced UPR^{mt}
206 and induced mitophagy. To further analyze the role of SGK-1 in mitochondrial
207 homeostasis we investigated how different mitochondrial perturbations affect SGK-1
208 protein levels during aging. Under basal conditions, SGK-1 protein expression levels
209 decreased during aging, from day 1 to day 10 (Figure 2A). Under strong mitochondrial
210 stress, such as PHB depletion or paraquat (PQ) treatment, SGK-1 levels were lower at
211 day 1 compared to control animals. At the end of the reproductive period (day 5), the
212 difference in the expression levels between control and *phb-1(RNAi)* treated worms was
213 eliminated, while the expression of SGK-1 upon PQ treatment was higher relative to the
214 control. However, in aged worms (day 10), SGK-1 expression levels increased upon
215 mitochondrial perturbation (Figure 2A). We then tested how SGK-1 protein levels
216 respond to mitochondrial quality control mechanisms. Inhibition of the UPR^{mt} by *atfs-*
217 *1(RNAi)* and inhibition of mitophagy by *pink-1(RNAi)* increased SGK-1 protein levels
218 relative to control at all times tested (Figure 2B). These results show that expression of
219 SGK-1 responds to mitochondrial perturbations and is regulated in a different manner
220 during the reproductive period than during aging, depending on the severity of
221 mitochondrial dysfunction.

222 Because the UPR^{mt} and mitophagy are particularly active under mitochondrial stress, we
223 next studied the impact of depleting each mitochondrial quality control mechanism on
224 SGK-1 protein levels under severe mitochondrial stress. In PHB-depleted worms, while
225 inhibiting the UPR^{mt} increased SGK-1 protein levels at day 1, day 5 and day 10, inhibiting
226 mitophagy only increased SGK-1 protein levels at day 1 (Figure 2C). In addition, we
227 pharmacologically induced mitochondrial stress with PQ. In this case, inhibition of
228 mitophagy did not influence SGK-1 expression, whereas inhibition of the UPR^{mt} caused
229 a dramatic increase of SGK-1 levels at day 5 and day 10 (Figure 2D). Moreover, the
230 observed reduction of SGK-1 expression during aging was abolished, as revealed by the
231 continuous increment in SGK-1 protein levels from day 1 to day 10 (Figure 2D). These
232 results show that under situations of strong mitochondrial stress the UPR^{mt} is more
233 relevant than mitophagy in the regulation of SGK-1 expression levels.

234 The high SGK-1 levels observed upon UPR^{mt} inhibition in situations of strong
235 mitochondrial stress during aging, could be related to the role of ATFS-1 in autophagy
236 induction. Autophagy is one of the compensatory pathways induced to protect cells from
237 severe mitochondrial defects [50] and has been suggested as a cytoprotective
238 mechanism implicated in the lifespan extension of *sgk-1* mutants upon prohibitin
239 depletion [14]. Thus, in the absence of ATFS-1, SGK-1 might be more necessary to keep
240 an efficient autophagy flux, as it has been previously proposed [28, 29]. Supporting this
241 hypothesis depleting genes involved in different steps of autophagy, such as initiation,
242 *unc-51(RNAi)* or nucleation, *bec-1(RNAi)*, increased SGK-1 protein levels, although the
243 increment was only significant at day 5 (Figure S4).

244 **A transcription factor RNAi screen identifies membrane sterols and lipid**
245 **homeostasis as modulators of the UPR^{mt} in TORC2/SGK-1 mutant.**

246 We reasoned that transcription factors whose depletion reduce the induction of the

247 UPR^{mt} in *sgk-1* mutants might be implicated in the activation of different pro-survival
248 pathways responsible for the long lifespan conferred by PHB depletion to TORC2
249 mutants [14]. Several transcription factors have been involved in the maintenance of
250 mitochondrial homeostasis and lifespan, including DAF-16, SKN-1, HIF-1 and HSF-1
251 [34, 40, 51-58]. Moreover, the UPR^{mt} promotes longevity by activating HIF-1, DAF-16
252 and SKN-1 [58]. We checked the involvement of these transcription factors in the
253 activation of the UPR^{mt} in *sgk-1* mutants and the essential TORC2 component *rict-1.*
254 Lack of DAF-16 further induced the mitochondrial stress in wild type animals (Figure 3A).
255 However, in *rict-1* mutant depletion of all the transcription factors enhanced the UPR^{mt}
256 (Figure S5), while only HIF-1 depletion did in *sgk-1* mutants (Figure 3A). This suggests
257 that TORC2 deficiency modulates the UPR^{mt} through additional kinases apart from *sgk-*
258 *1*. Nevertheless, depletion of none of the transcription factors tested inhibited the
259 expression of *hsp-6*, suggesting that different mechanisms are implicated in the UPR^{mt}
260 in TORC2/SGK-1 mutants.

261 With the aim of understanding the mechanism by which SGK-1 might regulate
262 mitochondrial function, and possibly aging, we performed an RNAi screen. We knocked-
263 down 836 transcription factors of the *C. elegans* genome and quantified the expression
264 of the mitochondrial stress response reporter. We found 20 genes whose depletion
265 reduced the expression of P*hsp-6*::GFP in *sgk-1* mutants (FC $<$ 0.6) (Figure 3B). HIF-1
266 depletion did not increase P*hsp-6*::GFP (average FC 1.067) in our screen as when
267 assayed on plate (Figure 3A). One possible explanation is that liquid growing conditions
268 are energetically more demanding, metabolism is altered and the UPR^{mt} might be
269 differentially regulated [59]. We reasoned that transcription factors that genetically
270 interact with *sgk-1* should further reduce worm size. Because *hsp-6* expression
271 increases through development, we focused on those transcription factors that when
272 depleted reduced both the UPR^{mt} and size of *sgk-1* mutants (Figure 3C).

273 Interestingly, 2 of these candidates, *lin-40* and *ceh-20*, are involved in endocytic traffic
274 [60]. SGK-1 has been reported to be involved in endocytosis and membrane trafficking
275 in different models [61-64] which supports the validity of the screen.

276 Additionally, we identified several nuclear hormone receptors (NHRs), a family of ligand-
277 regulated transcription factors that are activated by steroid hormones, and that play vital
278 roles in the regulation of metabolism, reproduction, and development. Among them,
279 NHR-8, a nuclear hormone receptor that regulates cholesterol levels, fatty acid
280 desaturation and apolipoprotein production [65]. NHR-8 is required for dietary restriction-
281 mediated lifespan extension in *C. elegans* [66, 67] but also normal lifespan [65].
282 Cholesterol is essential for hormone signaling, membrane structure and dynamics and
283 general fat metabolism. Also related with cholesterol is SBP-1, the homologue of sterol
284 regulatory element binding protein SREBP-1. SREBPs are required to produce
285 cholesterol [68] and regulate the expression of lipogenic genes across phyla [69, 70].
286 Interestingly, mammalian mTORC2 activates lipogenesis through SREBP-1 in the liver
287 [71]. Similarly, in *C. elegans,* SBP-1 acts downstream of TOR and IIS pathways and it is
288 involved in determination of adult lifespan. Depletion of *sbp-1* does not affect lifespan of
289 wild type animals, but suppresses the increment of lifespan caused by pharmaceutical
290 inhibition of TGF-β and IIS signaling [72].

291 In sum, we identified transcription factors involved in sterol metabolism, lipogenesis and
292 lipid membrane biology, whose depletion further reduced the size of *sgk-1* mutants
293 (Figure 3C), indicating a genetic interaction in *C. elegans*. Combining mutations in genes
294 that perturb the same process should enhance the observed phenotypes. Loss of
295 function of SGK-1 reduces worm size, slows down development [31, 33] and induces the
296 UPR^{mt} [14]. Depletion of both, NHR-8 and SBP-1, exacerbated the phenotypes of *sgk-1*
297 mutants at the young adult stage, further reducing worm size and inducing the UPR^{mt}
298 (Figure 3D). As reported, SBP-1 depletion reduced the size of wild type animals [73] and

299 the same did depletion of NHR-8. However, while depletion of neither NHR-8 nor SBP-
300 1 affected development of wild type animals, it specifically slowed down the
301 developmental rate of *sgk-1* mutants (Figure S5B), indicating a synthetic interaction.
302 Moreover, depletion of both, NHR-8 and SBP-1, mimicked the induced UPR^{mt} observed
303 in *sgk-1* loss-of-function mutants (Figure 3D). Apart from sterol [24], ceramide and
304 sphingolipids are also key structural lipids of membranes that are regulated by
305 Ypk1/SGK-1 in yeast [23, 26, 74, 75] and regulate membrane trafficking in *C. elegans*
306 [76]. We targeted by RNAi *sptl-1,* a serine palmitoyl-CoA acyltransferase responsible for
307 the first committed step in *de novo* sphingolipid synthesis, and *cgt-3,* a ceramide
308 glucosyltransferase, previously shown to interact with SGK-1 [62]. Similar to NHR-8 and
309 SBP-1, depletion of SPTL-1 and CGT-3 induced the UPR^{mt} in otherwise wild type worms,
310 recapitulating the *sgk1* mutant phenotype (Figure S5C). As reported, *cgt-3* depletion
311 caused a very slow developmental phenotype in *sgk-1* mutants [62]. Depletion of *sptl-1*
312 caused a partial (30 to 50%) larval arrest in otherwise wild type animals, while 100% of
313 *sgk-1* mutants arrested development at the L3 stage, indicating a synthetic lethal
314 interaction (Figure S5D). Not being at the same developmental stage, *hsp-6* expression
315 levels cannot be compared, nonetheless, depletion of *sptl-1* and *cgt-3* seemed to further
316 induced the UPR^{mt} in *sgk-1* mutants (Figure S5D). These results together, show that
317 defective lipogenesis and/or altered cholesterol and sphingolipid metabolism causes
318 mitochondrial proteotoxic stress and that the UPR^{mt} observed in *sgk-1* mutants could
319 reflect altered lipid and sterol homeostasis.

320 **Lipogenesis and lipoprotein/yolk formation defects of *sgk-1* mutants are**
321 **suppressed by prohibitin depletion.**

322 SREBPs are master regulators of lipogenesis and undergo sterol-regulated export from
323 the ER to the Golgi [77, 78] where proteases release the transcriptionally active portion

324 [68]. Also, transport of ceramide from the ER to the Golgi is a crucial step in sphingolipid
325 biosynthesis [79]. Both, in *C. elegans* and mammalian models, SREBPs are regulated
326 in response to altered membrane lipid ratios through ARF1 and GBF1 [80], which
327 function in vesicular trafficking, lipid homoeostasis and organelle dynamics [81]. In *C.*
328 *elegans* GBF-1 localizes in close proximity to the Golgi and the ER-exit sites and is
329 required for secretion and integrity of both organelles [82]. GFB-1 and SGK-1 physically
330 associate, being GBF-1 required for proper localization of SGK-1 near the basolateral
331 membrane of intestinal cells [62]. Interestingly, ARF1 and GBF1 play an evolutionarily
332 conserved role in ER-mitochondria contact site functionality and lack of GBF-1 causes a
333 similar increase in mitochondrial size as *sgk-1* deletion in *C. elegans* ([83] and Figure 1B
334 and S1).

335 Thus, we used TEM to explore whether TORC2/SGK-1 plays a role in ER contacts and
336 ER-mitochondria contact sites. We analyzed *sgk-1* mutants at the beginning of the
337 reproductive period (day 1 of adulthood) and at day 5 of adulthood. We observed
338 protruding structures from the endoplasmic reticulum, resembling exit sites, which were
339 not observed in wild type animals, where the ER appeared compacted (Figure 4A,
340 highlighted in Figure S6, and Figure S7). Lipid droplets emanate from the ER [84] and
341 production and secretion of lipoproteins are regulated via the ER-to-Golgi intermediary
342 compartment (ERGIC) [85]. Protruding ER exit sites (ERES) could reflect defective lipid
343 droplet formation and/or defective ER to Golgi or Golgi to ER secretion. TEM images
344 showed increased number of Golgi vesicles and increased size of the Golgi system in
345 *sgk-1* mutants (Figure 4A, highlighted in Figure S6, and Supplementary figure S7). The
346 increased presence of ERES indicates impaired lipid droplet and lipoprotein biogenesis,
347 as evidenced by the reduced content of lipid and yolk observed in *sgk-1* mutants (Figure
348 4A)(also visible in Figure S1). This agrees with the role of SGK-1 in lipogenesis and
349 vitellogenesis in *C. elegans* [36, 86, 87]. Interaction of lipid droplets with yolk forming

350 particles and vacuoles also appeared altered at day 1 of adulthood and abnormal
351 myelinated structures were visible (Figure S7)(also visible in Figure S1). At day 5, the
352 number of ERES was reduced as compared to day 1 in *sgk-1* mutants, instead, small
353 ER-emanating lipid droplets and myelinated structures/defective autolysosomes
354 accumulate (Figure 4a)(also visible in Figure S1). These phenotypes could reflect
355 defective endomembrane biology in *sgk-1* mutants, in agreement with the proposed role
356 for *sgk-1* in membrane trafficking in *C. elegans* [62] and yeast [63, 88]. In addition, the
357 accumulation of ERES affects the proximity of ER membranes to mitochondria. In wild
358 type animals, the ER appeared compacted and close to mitochondria, while in *sgk-1*
359 mutants less ER was observed in contact with mitochondria in the intestine and in muscle
360 (Figure 4A and B, respectively and Figure S6). This phenotype agrees with the observed
361 localization of mTORC2 to mitochondria-associated ER membranes (MAM) and
362 defective MAM observed in liver-specific mTORC2/rictor KO mice [89].

363 These results support a key role of SGK-1 in membrane trafficking, plausibly through
364 affecting membrane lipid ratios and the formation of membrane contact sites, that could
365 explain all the observed phenotypes, defective mitochondrial function and defects on
366 lipid droplet and lipoprotein biogenesis. Since prohibitin depletion suppressed
367 mitochondrial defects of *sgk-1* mutants (Figure 1), we investigated if lack of the PHB
368 complex could suppress lipogenesis and yolk/lipoprotein accumulation. We analyzed
369 TEM sections at the beginning of the intestine, before and after the gonad turn, in 5 days
370 old animals (Figure 4C and Figure S8). *sgk-1* mutants were defective in lipid droplet
371 formation and vitellogenesis, as previously reported [36, 86]. In addition, little
372 accumulation of lipoprotein pools at the pseudocoelom was observed compared to wild
373 type and prohibitin depleted animals (Figure S8). Strikingly, depletion of the
374 mitochondrial PHB complex suppressed both, lipid droplet accumulation and yolk
375 production defects of *sgk-1* mutants (Figure 4C and Figure S8). Furthermore, *sgk-1*

376 mutants presented all described phenotypes in OP50, a different bacterial food source
377 (Figure S9). The phenotypes observed in OP50 bacteria included abnormal foci of
378 myelinated forms, defective lipid droplet formation and generally reduced lipid content
379 and yolk, as well as increased mitochondrial size.

380 Autophagosomes receive lipids from the ER, ERES, ERGIC, the Golgi apparatus, as
381 well as from mitochondria and ER-mitochondria contact sites [90]. Moreover, inhibition
382 of late stages of autophagy has been shown to prevent the conversion of intestinal lipids
383 into yolk and the accumulation of lipoprotein pools at the pseudocoelom [91]. Thus, our
384 TEM analysis strongly suggests that *sgk-1* mutants suffer from a blockage of the
385 autophagy flux.

386 **Impaired autophagy flux of *sgk-1* mutants is suppressed by prohibitin**
387 **depletion.**

388 SGK-1 has been shown to modulate autophagy both via induction and blockage of
389 autophagy [27-29, 35, 92, 93] and we observed an accumulation of abnormal
390 autophagosomes in *sgk-1* mutants (Figure 4A and Figure S7). Thus, we analyzed the
391 autophagic state in *sgk-1* mutants in the presence and in the absence of the PHB
392 complex.

393 With a view to quantify autophagy we used a strain carrying the intestinal autophagy
394 reporter P*nhx-2*::mCherry::LGG-1 [94] which shows a diffused cytoplasmic expression
395 pattern under basal conditions but under induced autophagy shows a punctate
396 expression pattern due to the recruitment of LGG-1 to the autophagosomes. We
397 classified the level of autophagy based on 5 different categories from very low (animals
398 with a completely diffused expression pattern) to very high (animals with big
399 aggregations of LGG-1 all along the intestine) (see Materials and Methods and Figure
400 S10A). We quantified autophagy immediately after the reproductive period (day 5), when

401 LGG-1 puncta are more obvious. *sgk-1* mutants showed an enhanced autophagy signal
402 compared to wild type animals (Figure 5A), as previously described in worms [35, 38].
403 While depletion of the PHB complex significantly increased LGG-1 puncta in otherwise
404 wild type worms, no additive effect was observed in *sgk-1* mutants upon *phb-1* depletion
405 (Figure 5A). We knocked down *unc-51,* an essential gene for autophagosome formation,
406 as a control to ensure the signal visualized in the transgenic line corresponds to
407 autophagy and not to mCherry aggregation. *unc-51(RNAi)* reduced the autophagic signal
408 under all tested conditions (Figure S10B).

409 To better analyze autophagy flux, we performed electron microscopy analysis at day 5
410 of adulthood at the beginning of the intestine (see materials and methods). Characteristic
411 structures of impaired autophagy flux observed in TEM images of *C. elegans* are
412 abnormal foci with myelinated membranes [95]. Myelinated forms including
413 multivesicular bodies, multilaminar bodies and myelinated membrane whorls were
414 clearly visible in *sgk-1(ok538)* mutants (Figure 5B). Quantification in the different
415 backgrounds (Figure 5B, bottom panel) showed that myelinated forms rarely appeared
416 in wild type and in *phb-1(RNAi)* treated worms, while they accumulated in *sgk-1* mutants.
417 Interestingly, the accumulation of myelinated forms in *sgk-1* mutants was suppressed
418 upon *phb-1(RNAi)* (Figure 5B). Altogether, the differences in LGG-1 expression pattern
419 and the accumulation of electro-dense particles, suggest that while autophagy is induced
420 in PHB depleted worms, both, induction of autophagy and an impairment in the
421 autophagic flux occurs in *sgk-1* mutants, as previously proposed in yeast [27-29].

422 We confirmed activation of autophagy in *sgk-1(ok538)* mutants by looking at the
423 subcellular localization of the transcription factor HLH-30/TFEB, a positive regulator of
424 autophagy, lysosome biogenesis and longevity [96, 97]. We observed increased nuclear
425 localization of HLH-30 in *sgk-1* mutants (Figure 5C). In order to confirm blockage of
426 autophagy in *sgk-1* mutants we pharmacologically suppressed autophagy adding

427 Bafilomycin A1 (BafA), an inhibitor of vacuolar type H^+-ATPases that prevents lysosomal
428 acidification causing a blockage of the autophagic flux [98]. Upon bafilomycin treatment,
429 wild type worms showed an increment of the signal (34% increment), which corresponds
430 to the accumulation of non-degraded autophagosomes (figure 5d). Although Bafilomycin
431 further increased the autophagy signal in *sgk-1* mutants (Figure 5D), this increment was
432 considerably lower than the one observed in wild type worms (11% vs 34%), showing a
433 partial blockage of the autophagic flux. To further confirm this blockage in *sgk-1* mutants
434 we used the dual-fluorescent protein reporter mCherry::GFP::LGG-1 that allows to
435 monitor autophagosomes (APs), double-membrane vesicles that engulf cytosolic cargo,
436 and autolysosomes (ALs), where degradation of cargo takes place after APs fuse with
437 lysosomes [99, 100] (Figure 5E). Under the acidic environment of ALs, GFP is quenched,
438 therefore, ALs appear as red punctae, while APs appear as yellow [green and red]
439 punctae. While in wild type animals most red puncta appeared also green, in *sgk-1*
440 mutants we found a large amount of only red and abnormal intestinal puncta (Figure 5E)
441 indicating an accumulation of ALs. The same was true for the hypodermis, where *sgk-1*
442 mutants presented more ALs than wild type worms (Figure S11A). Further demonstrating
443 a role of SGK-1 in maintaining the autophagic flux, we observed a completely diffused
444 expression pattern of intestinal mCherry::LGG-1 in worms overexpressing SGK-1 at day
445 5 of adulthood and suppression of the increased autophagosomes observed upon *phb-*
446 *1* depletion (Figure S11B). Because autophagy is required for the conversion of intestinal
447 lipids into yolk, the suppression of abnormal autophagic structures upon PHB depletion
448 agree with the suppression of both, lipid droplet and yolk accumulation defects of *sgk-1*
449 mutants upon PHB depletion.

450 **Autophagy and the UPR^{mt}, but not mitophagy, are required for the**
451 **enhanced longevity of *sgk-1* mutants upon PHB depletion**

452 We have shown that long-lived *sgk-1(ok538)* mutants and PHB depleted animals have
453 induced mitochondrial quality control mechanisms such as mitophagy and the UPR^{mt}
454 (Figure 1). Similarly, autophagy is induced in both *sgk-1* mutants and PHB depleted
455 animals, however, the autophagy defects of *sgk-1* mutants are suppressed by PHB
456 depletion (Figure 5). In addition, in the absence of the PHB complex, SGK-1 protein
457 levels increase upon inhibition of the UPR^{mt} but not inhibition of mitophagy (Figure 2).
458 Therefore, we investigated the requirement of autophagy as well as both mitochondrial
459 quality control mechanisms for the lifespan extension conferred by prohibitin depletion
460 to *sgk-1* mutants. Depletion of ATFS-1 did not affect lifespan of wild type animals (Figure
461 6A and Table S1) [101]. Surprisingly, even though prohibitin depleted worms and *sgk-*
462 *1(ok538)* have induced UPR^{mt}, inhibiting this process did not shorten their lifespan
463 (Figures 6A and 6B and Table S1). However, preventing the UPR^{mt} suppressed the
464 longevity of *sgk-1;phb-1(RNAi)* treated mutants down to wild type levels (Figure 6B and
465 Table S1). On the same direction, inhibiting autophagy by *unc-51(RNAi)* treatment did
466 not affect lifespan of *phb-1* depleted worms nor of *sgk-1(ok538)* mutants (Figures 6C,
467 6D and Table S1), while it shortened that of *sgk-1;phb-1(RNAi)* treated animals (Figure
468 6D and table S1), although to a lesser extent than inhibiting the UPR^{mt}. Treatment with
469 *unc-51(RNAi)* shortened the lifespan of wild type worms (Figure 6C, Table S1 and [102]).
470 Autophagy is divided in four different steps [103]: initiation, nucleation, elongation and
471 final fusion with lysosomes for lysis of the cargo. Likewise inhibition of initiation (*unc-*
472 *51(RNAi)*), inhibition of nucleation (*bec-1(RNAi)*) and inhibition of elongation (*atg-*
473 *16(RNAi)*) shortened lifespan of the *sgk-1;phb-1(RNAi)* treated mutants (Figure S12).
474 Therefore, we conclude that both mechanisms, autophagy and the UPR^{mt}, are required

475 for the enhanced longevity of *sgk-1(ok538)* mutants upon PHB depletion, plausibly
476 because the UPR^{mt} transcription factor is a positive regulator of autophagy.

477 We also assessed the requirement of mitophagy for the longevity of *sgk-1* mutants
478 caused by the absence of the mitochondrial PHB complex. Inhibition of mitophagy did
479 not affect lifespan of wild type worms (Figure 6E, Table S1 and [40]). Interestingly,
480 preventing mitophagy showed a beneficial effect on lifespan of PHB depleted worms and
481 *sgk-1* mutants (Figure 6E, 6F and table S1). However, in the case of *sgk-1;phb-1(RNAi)*
482 treated worms inhibition of mitophagy did not affect lifespan in most of the cases (Figure
483 6F) and increased lifespan in one case (Table S1). It seems counterintuitive that
484 mitophagy inhibition could be beneficial for lifespan as damaged mitochondria would
485 accumulate. In fact, inhibition of mitophagy has been described as shortening lifespan
486 of long lived mitochondrial mutants as well as mutants of the insulin receptor *daf-2* [40].
487 Since in this study we carried out double RNAi experiments, we wondered whether this
488 discrepancy in lifespan phenotypes was due to the different experimental procedure. By
489 performing lifespan analysis in *daf-2(e1370)* mutants depleted of *pink-1* using diluted
490 RNAi (Figure S13A and Table S1), we conclude that the observed beneficial effects of
491 mitophagy inhibition were not due to the experimental procedure since in our hands *pink-*
492 *1(RNAi)* shortened lifespan of *daf-2(e1370),* as reported [40]. DAF-2 and SGK-1 act in
493 parallel pathways in the regulation of the UPR^{mt} and prohibitin-mediated longevity [14].
494 We, therefore, assayed the effect of inhibiting mitophagy in *daf-2;sgk-1* double mutants
495 and identified that depletion of PINK-1 further increased the lifespan of *daf-2;sgk-1*
496 double mutants (Figure S13B and Table S1), suggesting that loss of function of *sgk-1*
497 reverts the requirement of mitophagy for lifespan extension. Interestingly, depletion of
498 PINK-1 in *daf-2* mutants shortened lifespan and increased SGK-1 protein levels during
499 aging (Figure S13C). On the contrary, PHB-1 depletion, which increases *daf-2* mutants'
500 lifespan [13], reduced SGK-1 protein levels (Figure S13C).

501 We confirmed the beneficial effects of preventing mitophagy in *sgk-1* and *phb-1* deficient
502 backgrounds depleting DCT-1, a mitophagy receptor acting downstream of PINK-1 [40].
503 Lack of DCT-1 increased the lifespan of PHB depleted worms and *sgk-1* mutants (Figure
504 S13D, S13E and Table S1) without affecting the lifespan of wild type worms (Figure
505 S13D and Table S1), thus recapitulating *pink-1(RNAi)* phenotypes. However, in the case
506 of *sgk-1;phb-1(RNAi)* treated mutants, the role of *dct-1* was not clear, as it increased
507 lifespan in one out of two replicates (Figure S13E and Table S1). These results show
508 that mitophagy can be beneficial for lifespan under certain conditions, but detrimental in
509 certain pre-conditioned mutants such as *sgk-1* and PHB depleted worms. What
510 determines mitophagy being beneficial or detrimental deserves further investigation.

511 Altogether, our results show that autophagy and the UPR^{mt} are required for the lifespan
512 extension conferred by PHB depletion while *pink-1* mediated mitophagy is not. In
513 addition, in PHB depleted animals, inhibition of the UPR^{mt} results in a remarkable
514 increase of SGK-1 levels during aging, while mitophagy inhibition does not. To better
515 understand the differential requirement of both mitochondrial quality control
516 mechanisms, UPR^{mt} and mitophagy, for the lifespan extension of *sgk-1* mutants upon
517 PHB depletion, we examined their contribution to the observed pool of autophagosomes
518 in *sgk-1* mutants, PHB depleted animals, and *sgk-1;phb-1(RNAi)* treated mutants (Figure
519 6G). When treating worms with *atfs-1(RNAi)* we observed a reduction in the autophagic
520 signal under all tested conditions (Figure 6G), as expected since ATFS-1 regulates
521 directly the expression of LGG-1 [104]. Treatment with *pink-1(RNAi)* reduced the
522 accumulation of autophagosomes in *phb-1(RNAi)* and in *sgk-1* mutants, meaning that
523 the signal observed in *phb-1(RNAi)* and in *sgk-1* mutants corresponds partially to
524 mitophagy (Figure 6G), which agrees with the observed increase in PINK-1 protein in
525 *phb-1(RNAi)* and *sgk-1(RNAi)* treated worms (Figure 1A). However, inhibiting mitophagy
526 in *sgk-1;phb-1(RNAi)* did not significantly reduce the autophagosome pool (Figure 6G).

527 Therefore, it is tempting to speculate that the mechanism by which PHB depletion
528 extends *sgk-1* mutants lifespan is by inducing the UPR^{mt}, which in turn induces general
529 autophagy in a TORC2 independent manner.

530 Discussion

531 Depletion of PHB, a multimeric ring-like complex sitting in the inner mitochondrial
532 membrane induces the mitochondrial unfolded protein response (UPR^{mt}) and shortens
533 lifespan in wild type worms. However, lack of PHB further enhances the lifespan of a
534 deletion mutant of the nutrient and growth factor responsive kinase SGK-1, and the
535 activation of the UPR^{mt} is reduced [14]. In this work, we analyzed the interaction between
536 SGK-1 and the mitochondrial PHB complex. Our results strongly suggest that
537 mitochondrial, lipogenic and autophagic defects of *sgk-1* mutants are caused by
538 defective ER function and that PHB depletion suppresses them by altering membrane
539 lipid composition at ER-mitochondria contact sites, where TORC2 localizes, having
540 ultimately a beneficial outcome for lifespan.

541 mTORC2 and SGK-1 have previously been shown to regulate mitochondrial function by
542 maintaining mitochondria-associated ER membrane (MAM) integrity [89] and SGK-1 has
543 been reported to localize to mitochondria upon stress [17]. More recently, SGK-1 has
544 been shown to phosphorylate VDAC1 at the outer mitochondrial membrane, inducing its
545 degradation [35]. The data we present here supports a role for SGK-1 in MAM integrity.
546 By electron microscopy we described bigger mitochondria in *sgk-1* mutants compared to
547 wild type (Figure 1B). However, no obvious mitochondrial fragmentation or severe cristae
548 defects could be observed as previously described [35]. This might be due to different
549 growing conditions or the different alleles used. Although both predicted to be null alleles,
550 *ok538* is a deletion mutant [15], while *mg455* is a nonsense mutation [31]. Nonsense
551 mutations have been recently shown to trigger compensatory mechanisms [105]. We

552 believe a more detailed analysis of the different TORC-2/SGK-1 alleles is required to
553 understand the different phenotypes observed. Similarly, and contrary to what has been
554 reported [35], we described that *sgk-1* mutants had a dramatic increase in oxygen
555 consumption and a very reduced reserve capacity (Figures 1C and 1D). A low reserve
556 capacity corresponds to the maximal usage of the mitochondrial capacity under normal
557 conditions, which can be due to mitochondrial defects that rescind the ability of the
558 mitochondria to function at their full potential, or to a continuous higher energy demand.
559 Yeast Ypk1 deficient cells have reduced mitochondrial membrane potential [26], which
560 could explain a higher oxygen consumption to build up a membrane potential. Our
561 observation is also consistent with the increased mitochondrial respiration rate observed
562 in mTORC2/rictor knockdown in mammalian cells [43]. Consistent with increased
563 respiration rate, *sgk-1* mutants had increased ROS levels (Figure 1G). Interestingly,
564 Ypk1 has been involved in both, maintenance and response to ROS levels [26]. Although
565 the molecular bases of the connection between ROS levels and TORC2/Ypk1 signaling
566 are unknown, a link with sphingolipids homeostasis has been proposed [26]. The authors
567 show that sphingolipids modulate suppression of ROS while sphingolipid depletion
568 activates Ypk1, via ROS signaling, that in turn functions as a positive regulator of
569 sphingolipid biosynthesis [26]. Sphingolipids are essential components of biological
570 membranes, that together with ceramides regulate intracellular trafficking, signaling and
571 stress responses. TORC2/Ypk1 activates sphingolipid and ceramide biosynthesis [23,
572 74]. Furthermore, sphingolipids levels modulate Ypk1 expression in a positive feedback
573 loop to respond to membrane stress [75] and to regulate cell growth [24, 25]. In *C.*
574 *elegans* SGK-1 has been proposed to regulate membrane trafficking through
575 sphingolipids [62]. We show here that depletion of *sptl-1* and *cgt-3*, key genes in the
576 synthesis of ceramides and sphingolipids, induced the UPR^{mt} as *sgk-1* deletion mutants
577 do (Figure S5C and [14]) and synthetically interact with *sgk-1* (Figure S5D and [62]).
578 Interestingly, in worms, sphingolipid biosynthesis has been previously related with the

579 UPR^{mt}, with phosphorylated sphingosine being required in mitochondria to activate the
580 UPR^{mt} [106]. Inhibition of sphingolipids biosynthesis reduces the induction of the UPR^{mt}
581 due to a lack of ceramide, since ceramide supplementation rescues *hsp-6* induction
582 [107]. Similarly, the PHB depletion-mediated UPR^{mt} induction is suppressed in *sgk-1*
583 mutants [14].

584 Further, our transcription factor RNAi screen uncovered the implication of membrane
585 sterol and lipid homeostasis in the UPR^{mt} induction triggered by SGK-1 deficiency (Figure
586 3B). Particularly interesting were NHR-8 and SBP-1/SREBP-1, considering the role of
587 Ypk1 in sphingolipid metabolism [23, 26, 74, 75] and membrane sterol distribution at
588 plasma membrane-endoplasmic reticulum contact sites [24]. Cholesterol and
589 sphingolipids are essential components of cell membranes and are essential for
590 membrane dynamics in the cell. Here we show that depletion of key transcription factors
591 involved in lipogenesis and cholesterol metabolism, NHR-8 and SBP-1 [65, 69, 70],
592 further enhance phenotypes associated to *sgk-1* mutants, including worm size reduction,
593 developmental delay, and induction of the UPR^{mt} (Figure 3D and S5). Similarly, impaired
594 vitellogenesis is also observed in both *nhr-8* and *sgk-1* mutants [36, 65, 87]. These
595 results show that altered lipogenesis or membrane cholesterol signaling contribute to
596 mitochondrial stress and might be common processes regulated by SGK-1, NHR-8 and
597 SBP-1. Mammalian mTORC2 activates lipogenesis through SREBP-1 in the liver [71].
598 Therefore, it is possible that deficiencies in building up cholesterol in *sgk-1* deficient
599 animals result in defective SREBP-1/SBP-1 activation. Moreover, cholesterol depletion
600 prevents SGK1 signaling in *Xenopus laevis* oocytes [108] and, in yeast, TORC2
601 signaling is regulated at membrane contact sites which facilitate the formation of
602 membrane domains composed of specialized lipids [109]. Our data, altogether, strongly
603 suggest that, also in *C. elegans*, SGK-1 plays a key role in membrane lipid composition
604 and sterol homeostasis and that organellar membrane contact sites could be modulated

605 by TORC2/SGK-1 to coordinate cellular stress responses.

606 Our TEM analysis showed that *sgk-1* mutants are defective in lipid droplet and
607 yolk/lipoprotein production, as well as pseudocelomic lipoprotein accumulation (Figure
608 4, S7 and S8) which is in concordance with the reduced lipid content and vitelogenesis
609 observed in *sgk-1* mutants [36, 86, 87] and with the regulation of lipogenesis by mTORC2
610 through SREBP1 [71]. Moreover, TORC2 in different systems has been linked to
611 functions in different membrane-contact sites (MCS) such as ER-plasma membrane [24]
612 and ER-mitochondria [89]. Our TEM analysis supports a role for SGK-1 in ER
613 homeostasis (Figure 4A and S6), in consonance with the induced UPR^{ER} observed in
614 *sgk-1(ok538)* mutants [62]. In addition, we observed that the ER was not as close to
615 mitochondria as in wild type animals, with areas in muscle cells in which no ER was
616 observed (Figure 4B). In agreement, in mammalian systems, mTORC2 regulates
617 mitochondrial physiology [43] by localizing to mitochondria-associated ER membrane
618 [89]. Our study thus, indicates that SGK-1 plays a role in ER-mitochondria MCS that is
619 evolutionarily conserved. The ER consists of an elaborate network of membranes that
620 extends throughout the whole cell, making contacts with all organelles in the cell and the
621 plasma membrane [110]. Therefore, ER defects probably transcend to all important roles
622 of the ER in membrane biology, as we observed in *sgk-1* mutants. These include
623 defective lipid droplet formation and lipoprotein/yolk production. Interestingly, we showed
624 that mitochondrial PHB dysfunction suppresses defects in lipogenesis and
625 yolk/lipoprotein production (Figure 4c and S8).

626 Additionally, we observed accumulation of myelinated structures/defective
627 autolysosomes during aging (Figure 4A), which suggested a blockage of the autophagic
628 flux, plausibly due to defective endomembrane interactions, as autophagosomes receive
629 lipids from essentially all organelles and organellar-contact sites [90]. We confirmed both
630 induction and blockage of autophagy in *sgk-1* mutants by different means (Figure 5).

631 Importantly, we identified a blockage of the autophagy flux in the last phase of
632 autophagy, degradation of the cargo (Figure 5E). This agrees with yeast data where
633 Ypk1 mutants show induced autophagy [29] and reduced autophagy flux [28]. Thus,
634 blockage of autophagy is conserved in mTORC2/SGK-1 mutants, contrary to what has
635 been proposed [35]. Interestingly, depletion of PHB in *sgk-1* mutants reduced the
636 accumulation of myelinated forms, again making the phenotype similar to the wild type
637 situation (Figure 5B). This is in line with findings in yeast, where autophagy is restored
638 to wild-type levels in *ypk1* deleted *rho0* cells under amino acid-starvation conditions [28].
639 Moreover, in relation with lipid homeostasis, ceramide synthesis has been involved in
640 autophagy regulation and lifespan extension [111-113]. Inhibition of sphingolipids
641 synthesis increases lifespan [113]. More in particular, depletion of ceramide synthase
642 genes induces autophagy and increases lifespan [111, 112]. These phenotypes
643 resemble the effect of *sgk-1* deletion in PHB depleted animals; reduced UPR^{mt} induction
644 and increased lifespan [14].

645 We further showed that the UPR^{mt} and general autophagy, but not mitophagy, play an
646 important role in PHB depleted *sgk-1* mutants. Inhibition of the UPR^{mt}, but not mitophagy,
647 increase SGK-1 protein levels in PHB depleted animals (Figure 2C). Similarly, autophagy
648 and the UPR^{mt}, but not mitophagy, are required for the lifespan extension conferred by
649 PHB depletion to *sgk-1* mutants (Figure 6, S13D, S13E and Table S1). And finally, the
650 UPR^{mt}/ATFS-1, but not mitophagy, contribute to the pool of autophagosomes in PHB-
651 depleted *sgk-1* mutants (Figure 6G). We hypothesize that inhibition of the UPR^{mt} mimics
652 inhibition of autophagy because ATFS-1 is a positive regulator of autophagy [104]. We
653 speculate that the main function of SGK-1 is to keep organelle membrane dynamics,
654 therefore maintaining an efficient autophagic flux. PHB depletion suppresses membrane
655 defects of *sgk-1* mutants, making autophagy and the UPR^{mt} beneficial and essential for
656 lifespan. In line with this, the observed increase of SGK-1 protein levels upon

657 mitochondrial stress (Figure 2A and 2B) could reflect a need to increase the autophagy
658 flux to maintain a healthy mitochondrial population. The increase of SGK-1 protein levels
659 is more pronounced when strong mitochondrial stress (*phb-1* depletion or PQ treatment)
660 is combined with UPR^{mt} inhibition but not mitophagy inhibition (Figure 2C and 2D). We
661 hypothesize that in such conditions, inhibition of autophagy by inhibiting ATFS-1, further
662 increases the need of SGK-1 to keep an efficient autophagic flux. However, under strong
663 mitochondrial stress, inhibition of mitophagy does not affect SGK-1 levels plausibly
664 because mitophagy inhibition does not confer a further stress, instead it might be
665 beneficial to reduce mitochondrial clearance when mitochondria are severely damaged
666 and biogenesis is impaired. In fact, mitophagy is detrimental for both, PHB and *sgk-1*
667 single mutants (Figures 6E, 6F and Table S1), while autophagy and the UPR^{mt} are not
668 relevant (Figure 6B, 6D and Table S1). Under highly energetically demanding conditions,
669 such as the reproductive period, severely damaged mitochondria (PHB depleted or PQ
670 treated) results in reduced SGK-1 levels probably to reduce the autophagic flux in order
671 to increase the mitochondrial population or to prevent the accumulation of defective
672 membranes that cannot efficiently contribute to autophagy. Further supporting a role for
673 SGK-1 in keeping the autophagic flux, inhibition of autophagy also results in increased
674 SGK-1 protein levels (Figure S4).

675 Elucidating the molecular mechanism of how lack of the PHB complex suppresses all
676 *sgk-1* mutants' deficiencies such as mitochondrial dysfunction, increased mitochondrial
677 size and cytosolic ROS, lipogenesis and yolk production defects and autophagy
678 blockage, deserves further investigation. But many observations suggest that ER-
679 mitochondria associated ER membranes, MAM, might be at play. MAM has been
680 proposed as a hub for mTORC2-Akt signaling [114] and TORC2/SGK1 plays a
681 conserved role in sphingolipid and ceramide biosynthesis [23, 25, 74, 75]. The main
682 function of MAM is to facilitate the transfer of lipids and calcium between the two

683 organelles [115, 116]. MAM also mediates ER homeostasis and lipid biosynthesis by
684 harboring chaperones and several key lipid synthesis enzymes [117, 118], including
685 synthesis and maturation of cholesterol, phospholipids and sphingolipids [119-122].
686 Besides, MAM of rat liver contains highly active sphingolipid-specific
687 glycosyltransferases [123], and ceramide metabolism has been proposed to occur at
688 mitochondria as well as at MAM [124]. The PHB complex affects membrane lipid
689 composition and genetically interacts with proteins involved in ER-mitochondria
690 communication. PHB has been proposed to play a key role as membrane organizer since
691 it affects the distribution of cardiolipin and phosphatidylethanolamine [3, 125, 126]. In
692 addition, lack of PHB in MEFs affects lipid metabolism and cholesterol biosynthesis
693 [127]. Moreover, PHB proteins have been genetically linked to the mitochondrial inner
694 membrane organizing system (MINOS) and to ER-mitochondria encountered structures
695 (ERMES) complexes in synthetic lethal screens in yeast, forming part of a large ER-
696 mitochondria organizing network, ERMIONE [125, 128, 129]. On the other hand, PHB
697 has been related with sphingosine metabolism as it interacts with sphigosine-1-
698 phosphate in mice mitochondria [130].

699 In the future, it will be important to decipher the role of SGK-1 at MAM and MCS at the
700 molecular level and the mechanism by which PHB depletion suppresses *sgk-1* defects.
701 It seems plausible that PHB deficiency could alter membrane lipid composition in a
702 favorable manner for *sgk-1* mutants. In that direction, it would be relevant to test if
703 sphingolipid metabolism, lipogenesis and lipoprotein production are required for the
704 lifespan increase that PHB depletion confers to *sgk-1* mutants.

705 Materials and Methods

706 ***C. elegans* strains and maintenance**

707 The *C. elegans* strains used in this study were: N2 (wild type); MRS486: *sgk-1(ok538)X*
708 (3x outcrossed from BR4774, in total 11x outcrossed to N2 from the CGC strain VC345;
709 MRS88: *daf-2(e1370)III;* MRS68: *daf-2(e1370)III;sgk-1(ok538)X;* MRS386: *byEx*[*Psgk-*
710 *1::*SGK-1*::*GFP *+ rol-6(su1006)* (1x outcrossed from BR2773 [15])*;* MRS38: *daf-*
711 *2(e1370)III;byEx[*P*sgk-1::*SGK-1::GFP *+ rol-6(su1006)];* VK1093: *vkEx1093[*P*nhx-*
712 *2::*mCherry::LGG1]; MRS92: *sgk-1(ok538)X;vkEx1093[*P*nhx-2::*mCherry::LGG1];
713 MRS112: *byEx[*P*sgk-1::*SGK-1::GFP *+ rol-6(su1006)]; vkEx1093[*P*nhx-*
714 *2::*mCherry::LGG1]; SJ4100: *zcIs13[*P*hsp-6::*GFP*]V;* MRS19: *sgk-*
715 *1(ok538)X;zcIs13[*P*hsp-6::*GFP*]V;* MRS63: *rict-1(ft7)II;zcIs13[*P*hsp-6::*GFP*]V*; BR4006:
716 *pink-1(tm1779)II;byEx655[*P*pink-1::*PINK-1::GFP + P*myo-2::*mCherry + herring sperm
717 DNA]; MAH215: *sqIs11*[P*lgg-1*::mCherry::GFP::LGG-1 + *rol-6(su1006)*]; MRS555: *sgk-*
718 *1(ok538)X;sqIs11*[P*lgg-1*::mCherry::GFP::LGG-1 + *rol-6(su1006)*]; MAH240:
719 *sqIs17*[P*hlh-30*::HLH-30::GFP + *rol-6(su1006)*]; MRS558: *sgk-1(ok538)X;sqIs17*[P*hlh-*
720 *30*::HLH-30::GFP + *rol-6(su1006)*]; MRS505: *sod-1(tm776)II* (2x outcrossed to N2);
721 MRS516: *sod-1(tm776)II;sgk-1(ok538)X*; MRS504: *sod-2(gk257)I* (2x outcrossed to N2);
722 MRS510: *sod-2(gk257)I;sgk-1(ok538)X*.

723 Unless otherwise stated, we cultured the worms according to standard methods [131].
724 We maintained nematodes at 20°C on nematode growth media (NGM) agar plates
725 seeded with live *Escherichia coli* OP50 (obtained from the CGC).

726 **RNAi assays on plates**

727 For RNAi experiments worms were placed on NGM plates, supplemented with 25 μg/ml
728 carbenicillin (Sigma-Aldrich) and 10 μg/ml nystatin (Sigma-Aldrich), seeded with HT115
729 (DE3) *Escherichia coli* bacteria (deficient for RNase-E) transformed with empty vector
730 (control) or the required target gene RNAi construct. Each bacterial strain was
731 inoculated, from an overnight pre-inoculum, in LB (ampicillin (100 μg/ml) (Sigma-Aldrich)

732 and tetracycline (15 μg/ml) (Sigma-Aldrich). The overnight culture was diluted (1:10) and
733 grown in a shaking incubator at 37°C for 3 hours, until it reached an OD_{600} of around 1.5.
734 Then, in order to induce the dsRNA expression, we added IPTG (final concentration: 1
735 mM) (Sigma-Aldrich) to the bacterial culture and we harvested the bacterial culture after
736 2 hours of incubation at 37°C by centrifugation (8 min at 6000×*g,* 4°C). Following, we
737 washed the pellets with S Basal and harvested them again. Finally, we re-suspended
738 bacterial pellets to a final concentration of 30 g/l in complete S Medium. Bacterial stocks
739 were kept at 4°C up to 4 days before being used. For all the RNAi treatments, bacterial
740 stocks were mixed in a proportion of 1:1 before seeding the plates.

741 A semi-synchronous embryo population was grown on plates seeded with the
742 appropriate RNAi bacterial clone at 20°C until the desired stage (young adult, day 1, day
743 5 or day 10 of adulthood). During the egg-laying period, we transferred worms every day
744 and every 2 days thereafter.

745 To pharmacologically induce a strong mitochondrial stress, we transferred L3 to fresh
746 RNAi plates containing 0.25 mM Paraquat (Sigma-Aldrich).

747 **Imaging**

748 On the day of imaging, worms were anesthetized with 10 mM Levamisole (Sigma-
749 Aldrich) or with a mixture of 10 mM Levamisole and 5 mM NaN_3 (Sigma-Aldrich) for
750 confocal imaging and mounted on 2% agarose pads. P*pink-1::*PINK-1::GFP, P*nhx-*
751 *2::*mCherry::LGG1 and P*sgk-1::*SGK-1::GFP reporter were observed using the AxioCam
752 MRm camera on a Zeiss ApoTome Microscope; P*lgg-1*::mCherry::GFP::LGG-1 reporter
753 was imaged with a confocal Nikon A1R equipped with a Plan Apo VC 60x/1.4 objective
754 and P*hsp-6::*GFP animals were visualized with a Leica M205 Stereoscope equipped with
755 a Plan Apo 5.0x/0.50 LWD objective and a ORCA-Flash4.0 LT Hamamatsu digital
756 camera.

757 Image analysis was performed using the ImageJ software. Emission intensity was
758 measured on greyscale images with a pixel depth of 16 bits. At least two independent
759 assays were carried out and the combined data was analyzed using the GraphPad Prism
760 software (version 5.0a).

761 **Electron microscopy**

762 Transmission electron microscopy (TEM) of *C. elegans* was carried out as described
763 [132] with small modifications. Adult worms, at day 1 or 5, were immersed in 0.8%
764 glutaraldehyde + 0.8% osmium tetroxide in 0.1 M sodium cacodylate buffer, pH7.4.
765 Carefully, under a dissecting scope, we cut the animals with a scalp at the posterior end
766 of the intestine, removing the tail, and kept the samples for 1 hour on ice under dark
767 conditions to allow complete penetration of the fixing solution. We washed the worms
768 three times with 0.1 M sodium cacodylate buffer and fixed them over night at 4°C in 2%
769 osmium tetroxide in 0.1 M sodium cacodylate buffer; the entire procedure was performed
770 on ice. On the next day, we washed the worms three times with 0.1 M sodium cacodylate
771 buffer on ice and finally embedded the worms in small cubes of 1% agarose. We then
772 dehydrated the samples by incubating them in 50%, 70% and 90% ethanol for 10
773 minutes each, followed by 3 washes of 10 minutes each in 100% ethanol, at room
774 temperature. Next, we incubated the samples in a 50:50 ethanol/propylene oxide
775 solution for 15 minutes followed by 2 incubations of 15 minutes each in 100% propylene
776 oxide. We then infiltrated the samples on a rotator or with an embedding machine for 2
777 hours in a 3:1 ratio of propylene oxide to resin and next for 2 hours in a 1:3 ratio of
778 propylene oxide to 3 resin. Following, we incubated the samples overnight in 100% resin
779 and the next day changed to fresh 100% resin for 4 hours. We finally arranged the
780 samples in a flat embedding mold and cured them at 60°C for 2 days.

781 We cut the worms at the level of the first intestinal cells, immediately before and after the
782 gonad turn, specifically at 175 μm, 185 μm, 250 μm and 350 μm from the mouth.

783 For myelinated forms quantification, we analyzed 12 areas of 56 μm^2 per condition and
784 counted together multivesicular bodies (MVB), multillaminar bodies (MLB) and
785 myelinated forms. Data was analyzed using the GraphPad Prism software (version 5.0a).

786 **Oxygen consumption**

787 Worm oxygen consumption was measured using the Seahorse XFp Analyzer (Agilent)
788 as described [133]. Briefly, worms at the young adults stage (30 per well) or day 6
789 adult worms (20 per well), were transferred into M9-filled Seahorse plates. OCR was
790 measured 8 times in basal conditions as well as after each injection. Working solutions
791 were diluted in M9 at the final concentrations: FCCP (Sigma-Aldrich) 250 µM,
792 oligomycin (Sigma-Aldrich) 250 µM and NaN_3 (Sigma-Aldrich) 400 mM. Data were
793 normalized by the protein content quantified by the bicinchoninic acid assay
794 (Thermofsiher). The OCR values were arranged in order to see the response to the
795 drug. Basal OCR corresponded to the average of the 8 measurements under basal
796 conditions, while the rest of the values derived from the average of the last 4
797 measurements. At least three independent assays were carried out and the combined
798 data was analyzed by *t*-test using GraphPad Prism software (version 5.0a).

799 **Quantification of Reactive oxygen species**

800 Cytoplasmic ROS was quantified using 2,7-dichlorofluorescin-diacetate (H2-DCFDA)
801 dye (Sigma-Aldrich) modified from [13]. Briefly, 150 nematodes at the young adult stage
802 were manually selected and recovered in M9 buffer to a final concentration of 1 worm/µl.
803 50 µl of the worm suspension was transferred into a 96-well flat bottom plate in triplicate
804 (Thermo Fisher Scientific) and 50 µl of 100uM H2-DCF-DA solution was added to the

805 wells (H2-DCF-DA to a final concentration of 50 μM). Immediately, basal fluorescence
806 was measured (T_o) (Ex/Em: 485/520 nm) using a microplate reader (PolarStar Omega.
807 BMG, LabTech). After 1 hour of incubation at 20 ºC shaking, fluorescence was measure
808 one again (T_1). The final fluorescence was calculated by T_1-T_0. Data were normalized
809 by the protein content quantified by the bicinchoninic acid assay (BCA) (Thermo
810 Fisher Scientific) and manually counting the number of worms per well. At least three
811 independent assays were carried out and the combined data was analyzed by *t*-test
812 using GraphPad Prism software (version 5.0a).

813 **Protein Content Quantification**

814 Total protein content was determined using the bicinchoninic acid (BCA) method.
815 Briefly, pellets from 50 worms were dried in a Speed Vac Concentrator (SPD12 1P
816 SpeedVac, Thermo Scientific), 20 μl of 1 M NaOH were added to the dry pellet. Fat
817 was degraded by heating at 70°C for 25 min and 180 μl of distilled water was added.
818 After vortexing, the tubes were centrifuged at 14000 rpm for 5 min and 25 μl of the
819 supernatant were transferred into a 96 well plate. Next, 200 μl of the BCA reagent,
820 prepared according to manufacturer's instructions (Pierce BCA Protein Assay Kit,
821 Thermo Scientific) was added to the sample. After incubation at 37°C for 30 min, the
822 plate was cooled to room temperature and absorbance was measured using the
823 POLARstar Omega luminometer (BGM Labtech) at 560 nm.

824 **Autophagy assays**

825 In order to monitor autophagy in *C. elegans* we used the reporter strain Ex[*Pnhx-*
826 *2*::mCherry::LGG-1] [94]. Animals were classified in 5 different expression categories
827 (Supplementary figure S10): Very low: animals with a completely diffused expression
828 pattern; Low: animals with a generally diffuse expression pattern but with the presence
829 of small puncta; Medium: animals with puncta along the intestine; High: animals showing

830 aggregation of LGG-1 puncta mostly in the posterior part of the intestine; Very high:
831 animals with large LGG-1 aggregates along the whole intestine. To avoid bias in the
832 classification process, different researchers performed blind scoring on the same animal
833 images and disputes were resolved after discussion.

834 To determine whether increased levels of LGG-1 puncta corresponded to induced
835 autophagy or a blockage in the flux, we treated day 5 adult worms with Bafilomycine A_1
836 (BafA; Sigma-Aldrich), which blocks lysosome acidification. Animals were washed from
837 plates with M9 buffer and harvested in 15 ml tubes. In order to remove excess of bacteria,
838 we washed animals at least three times with M9 by letting the worms to settle at the
839 bottom of the tubes and then removed the supernatant. After washes, worms were
840 incubated for 6 hours in M9 with BafA (1.6 mM) or DMSO (1.5%) at 20°C with agitation.

841 At least 3 independent assays were carried out and the combined data was analyzed by
842 *t-test* using GraphPad Prism software (version 5.0a).

843 **Lifespan Analysis**

844 All lifespans were performed at 20°C. Semi-synchronized eggs were obtained by
845 hypochlorite treatment of adult hermaphrodites and placed on NGM plates seeded with
846 HT115 *E. coli* bacteria. During the course of the lifespan assays, we transferred adult
847 worms to fresh plates every day during their reproductive period and afterwards on
848 alternate days. Worms were scored as dead when they no longer responded to touch,
849 while exploded animals, those exhibiting bagging (embryo hatching inside the worm), or
850 dried out at the edges of the plates were censored.

851 For N-Acetyl-L-Cysteine (NAC) (Sigma-Aldrich) treatments we added NAC to the RNAi
852 medium to a final concentration of 8 mM.

853 We used the GraphPad Prism software (version 5.0a) to plot survival curves and to

854 determine significant differences in lifespans (log-rank (Mantel-Cox) test). See Table S1
855 for lifespan statistics.

856 **RNAi screen**

857 We performed an image-based RNAi screen as previously described[12]. Briefly, we
858 dispensed synchronized *sgk-1(ok538);*P*hsp-6*::GFP L1 larvae in 96 well plates using a
859 microplate dispenser (EL406 washer dispenser, BioTek) and added the corresponding
860 dsRNA encoding bacterial culture. Next, we incubated the worms at 20ºC with constant
861 shaking (120 rpm - New Brunswick™ Innova® 44/44R) until they reached the young adult
862 stage. We acquired pictures of each well using the IN Cell Analyzer 2000 (GE
863 Healthcare) and performed the image analysis with a user-defined protocol which was
864 developed on the Developer Toolbox software (GE Healthcare). We tested 836 RNAi
865 clones in duplicate and candidates were defined based on the adjusted *p* value and the
866 fold change (FC) (P value < 0.001 and FC < 0.6).

867 ## Acknowledgements

868 Some strains were provided by the Caenorhabditis Genetics Center (CGC), which is
869 funded by NIH Office of Research Infrastructure Programs (P40 OD010440). Special
870 thanks to Ralf Baumeister (Albert-Ludwig University, Germany) for the strain
871 BR2773:*byEx*[*Psgk-1::*SGK-1*::*GFP] [15] and to Nuria Flames for sharing her
872 transcription factor RNAi library. Thanks to Mario Soriano Navarro for technical help with
873 TEM. M.A-S was supported by the Ramón y Cajal program of the Spanish Ministerio de
874 Economía y Competitividad (MINECO), RYC-2010-06167. B.H.R. was supported by the
875 Spanish MINECO FPI program, BES-2013-064047. Our work is supported by the
876 Spanish Ministerio de Economía y Competitividad (BFU2012-35509), and the European
877 Research Council (ERC-2011-StG-281691).

878 ## Author contributions

879 B.H.R., M.M.P.J. and M.A.-S. designed the experiments; B.H.R., M.M.P.J., M.J.R.-P.
880 A.P., M.D.M.-B. P.dl.C.R., R.G. and M.A.-S. carried out experiments; B.H.R., M.M.P.J.,
881 M.J.R.-P. A.P., M.D.M.-B. P.dl.C.R., R.G. and M.A.-S analyzed the data and interpreted
882 results and B.H.R. and M.A.-S wrote the manuscript. All authors read, commented and
883 approved the final manuscript.

884 ## Competing interests

885 The authors declare no competing financial interests.

886 ## References

887 1. Merkwirth, C., and Langer, T. (2009). Prohibitin function within mitochondria: essential roles
888 for cell proliferation and cristae morphogenesis. Biochim Biophys Acta *1793*, 27-32.
889 2. Artal-Sanz, M., and Tavernarakis, N. (2009). Prohibitin and mitochondrial biology. Trends
890 Endocrinol Metab *20*, 394-401.
891 3. Osman, C., Haag, M., Potting, C., Rodenfels, J., Dip, P.V., Wieland, F.T., Brugger, B.,
892 Westermann, B., and Langer, T. (2009). The genetic interactome of prohibitins: coordinated
893 control of cardiolipin and phosphatidylethanolamine by conserved regulators in
894 mitochondria. J Cell Biol *184*, 583-596.
895 4. Artal-Sanz, M., Tsang, W.Y., Willems, E.M., Grivell, L.A., Lemire, B.D., van der Spek, H.,
896 and Nijtmans, L.G. (2003). The mitochondrial prohibitin complex is essential for embryonic
897 viability and germline function in Caenorhabditis elegans. J Biol Chem *278*, 32091-32099.
898 5. Nijtmans, L.G., Artal, S.M., Grivell, L.A., and Coates, P.J. (2002). The mitochondrial PHB
899 complex: roles in mitochondrial respiratory complex assembly, ageing and degenerative
900 disease. Cell Mol Life Sci *59*, 143-155.
901 6. Thuaud, F., Ribeiro, N., Nebigil, C.G., and Desaubry, L. (2013). Prohibitin ligands in cell
902 death and survival: mode of action and therapeutic potential. Chem Biol *20*, 316-331.
903 7. Nijtmans, L.G., de Jong, L., Artal Sanz, M., Coates, P.J., Berden, J.A., Back, J.W., Muijsers,
904 A.O., van der Spek, H., and Grivell, L.A. (2000). Prohibitins act as a membrane-bound
905 chaperone for the stabilization of mitochondrial proteins. EMBO J *19*, 2444-2451.
906 8. Merkwirth, C., Martinelli, P., Korwitz, A., Morbin, M., Bronneke, H.S., Jordan, S.D., Rugarli,
907 E.I., and Langer, T. (2012). Loss of prohibitin membrane scaffolds impairs mitochondrial
908 architecture and leads to tau hyperphosphorylation and neurodegeneration. PLoS Genet *8*,
909 e1003021.
910 9. Wei, Y., Chiang, W.C., Sumpter, R., Jr., Mishra, P., and Levine, B. (2017). Prohibitin 2 Is an
911 Inner Mitochondrial Membrane Mitophagy Receptor. Cell *168*, 224-238 e210.
912 10. Yoneda, T., Benedetti, C., Urano, F., Clark, S.G., Harding, H.P., and Ron, D. (2004).
913 Compartment-specific perturbation of protein handling activates genes encoding
914 mitochondrial chaperones. J Cell Sci *117*, 4055-4066.
915 11. Benedetti, C., Haynes, C.M., Yang, Y., Harding, H.P., and Ron, D. (2006). Ubiquitin-like
916 protein 5 positively regulates chaperone gene expression in the mitochondrial unfolded
917 protein response. Genetics *174*, 229-239.
918 12. Hernando-Rodriguez, B., Erinjeri, A.P., Rodriguez-Palero, M.J., Millar, V., Gonzalez-
919 Hernandez, S., Olmedo, M., Schulze, B., Baumeister, R., Munoz, M.J., Askjaer, P., et al.

(2018). Combined flow cytometry and high-throughput image analysis for the study of essential genes in Caenorhabditis elegans. BMC Biol *16*, 36.
13. Artal-Sanz, M., and Tavernarakis, N. (2009). Prohibitin couples diapause signalling to mitochondrial metabolism during ageing in C. elegans. Nature *461*, 793-797.
14. Gatsi, R., Schulze, B., Rodriguez-Palero, M.J., Hernando-Rodriguez, B., Baumeister, R., and Artal-Sanz, M. (2014). Prohibitin-mediated lifespan and mitochondrial stress implicate SGK-1, insulin/IGF and mTORC2 in C. elegans. PLoS One *9*, e107671.
15. Hertweck, M., Gobel, C., and Baumeister, R. (2004). C. elegans SGK-1 is the critical component in the Akt/PKB kinase complex to control stress response and life span. Dev Cell *6*, 577-588.
16. Brickley, D.R., Agyeman, A.S., Kopp, R.F., Hall, B.A., Harbeck, M.C., Belova, L., Volden, P.A., Wu, W., Roe, M.W., and Conzen, S.D. (2013). Serum- and glucocorticoid-induced protein kinase 1 (SGK1) is regulated by store-operated Ca2+ entry and mediates cytoprotection against necrotic cell death. J Biol Chem *288*, 32708-32719.
17. O'Keeffe, B.A., Cilia, S., Maiyar, A.C., Vaysberg, M., and Firestone, G.L. (2013). The serum- and glucocorticoid-induced protein kinase-1 (Sgk-1) mitochondria connection: identification of the IF-1 inhibitor of the F(1)F(0)-ATPase as a mitochondria-specific binding target and the stress-induced mitochondrial localization of endogenous Sgk-1. Biochimie *95*, 1258-1265.
18. Bell, L.M., Leong, M.L., Kim, B., Wang, E., Park, J., Hemmings, B.A., and Firestone, G.L. (2000). Hyperosmotic stress stimulates promoter activity and regulates cellular utilization of the serum- and glucocorticoid-inducible protein kinase (Sgk) by a p38 MAPK-dependent pathway. J Biol Chem *275*, 25262-25272.
19. Leong, M.L., Maiyar, A.C., Kim, B., O'Keeffe, B.A., and Firestone, G.L. (2003). Expression of the serum- and glucocorticoid-inducible protein kinase, Sgk, is a cell survival response to multiple types of environmental stress stimuli in mammary epithelial cells. J Biol Chem *278*, 5871-5882.
20. Webster, M.K., Goya, L., Ge, Y., Maiyar, A.C., and Firestone, G.L. (1993). Characterization of sgk, a novel member of the serine/threonine protein kinase gene family which is transcriptionally induced by glucocorticoids and serum. Mol Cell Biol *13*, 2031-2040.
21. Perrotti, N., He, R.A., Phillips, S.A., Haft, C.R., and Taylor, S.I. (2001). Activation of serum- and glucocorticoid-induced protein kinase (Sgk) by cyclic AMP and insulin. J Biol Chem *276*, 9406-9412.
22. Di Cristofano, A. (2017). SGK1: The Dark Side of PI3K Signaling. Curr Top Dev Biol *123*, 49-71.
23. Muir, A., Ramachandran, S., Roelants, F.M., Timmons, G., and Thorner, J. (2014). TORC2-dependent protein kinase Ypk1 phosphorylates ceramide synthase to stimulate synthesis of complex sphingolipids. Elife *3*.
24. Roelants, F.M., Chauhan, N., Muir, A., Davis, J.C., Menon, A.K., Levine, T.P., and Thorner, J. (2018). TOR complex 2-regulated protein kinase Ypk1 controls sterol distribution by inhibiting StARkin domain-containing proteins located at plasma membrane-endoplasmic reticulum contact sites. Mol Biol Cell *29*, 2128-2136.
25. Lucena, R., Alcaide-Gavilan, M., Schubert, K., He, M., Domnauer, M.G., Marquer, C., Klose, C., Surma, M.A., and Kellogg, D.R. (2018). Cell Size and Growth Rate Are Modulated by TORC2-Dependent Signals. Curr Biol *28*, 196-210 e194.
26. Niles, B.J., Joslin, A.C., Fresques, T., and Powers, T. (2014). TOR complex 2-Ypk1 signaling maintains sphingolipid homeostasis by sensing and regulating ROS accumulation. Cell Rep *6*, 541-552.
27. Vlahakis, A., Graef, M., Nunnari, J., and Powers, T. (2014). TOR complex 2-Ypk1 signaling is an essential positive regulator of the general amino acid control response and autophagy. Proc Natl Acad Sci U S A *111*, 10586-10591.
28. Vlahakis, A., Lopez Muniozguren, N., and Powers, T. (2016). Calcium channel regulator Mid1 links TORC2-mediated changes in mitochondrial respiration to autophagy. J Cell Biol *215*, 779-788.
29. Vlahakis, A., Lopez Muniozguren, N., and Powers, T. (2017). Stress-response transcription factors Msn2 and Msn4 couple TORC2-Ypk1 signaling and mitochondrial respiration to ATG8 gene expression and autophagy. Autophagy *13*, 1804-1812.

30. Mizunuma, M., Neumann-Haefelin, E., Moroz, N., Li, Y., and Blackwell, T.K. (2014). mTORC2-SGK-1 acts in two environmentally responsive pathways with opposing effects on longevity. Aging Cell *13*, 869-878.
31. Soukas, A.A., Kane, E.A., Carr, C.E., Melo, J.A., and Ruvkun, G. (2009). Rictor/TORC2 regulates fat metabolism, feeding, growth, and life span in Caenorhabditis elegans. Genes Dev *23*, 496-511.
32. Chen, A.T., Guo, C., Dumas, K.J., Ashrafi, K., and Hu, P.J. (2013). Effects of Caenorhabditis elegans sgk-1 mutations on lifespan, stress resistance, and DAF-16/FoxO regulation. Aging Cell *12*, 932-940.
33. Jones, K.T., Greer, E.R., Pearce, D., and Ashrafi, K. (2009). Rictor/TORC2 regulates Caenorhabditis elegans fat storage, body size, and development through sgk-1. PLoS Biol *7*, e60.
34. Tullet, J.M., Hertweck, M., An, J.H., Baker, J., Hwang, J.Y., Liu, S., Oliveira, R.P., Baumeister, R., and Blackwell, T.K. (2008). Direct inhibition of the longevity-promoting factor SKN-1 by insulin-like signaling in C. elegans. Cell *132*, 1025-1038.
35. Zhou, B., Kreuzer, J., Kumsta, C., Wu, L., Kamer, K.J., Cedillo, L., Zhang, Y., Li, S., Kacergis, M.C., Webster, C.M., et al. (2019). Mitochondrial Permeability Uncouples Elevated Autophagy and Lifespan Extension. Cell *177*, 299-314 e216.
36. Dowen, R.H., Breen, P.C., Tullius, T., Conery, A.L., and Ruvkun, G. (2016). A microRNA program in the C. elegans hypodermis couples to intestinal mTORC2/PQM-1 signaling to modulate fat transport. Genes Dev *30*, 1515-1528.
37. Dillin, A., Hsu, A.L., Arantes-Oliveira, N., Lehrer-Graiwer, J., Hsin, H., Fraser, A.G., Kamath, R.S., Ahringer, J., and Kenyon, C. (2002). Rates of behavior and aging specified by mitochondrial function during development. Science *298*, 2398-2401.
38. Lehmann, S., Bass, J.J., and Szewczyk, N.J. (2013). Knockdown of the C. elegans kinome identifies kinases required for normal protein homeostasis, mitochondrial network structure, and sarcomere structure in muscle. Cell Commun Signal *11*, 71.
39. Kirienko, N.V., Ausubel, F.M., and Ruvkun, G. (2015). Mitophagy confers resistance to siderophore-mediated killing by Pseudomonas aeruginosa. Proc Natl Acad Sci U S A *112*, 1821-1826.
40. Palikaras, K., Lionaki, E., and Tavernarakis, N. (2015). Coordination of mitophagy and mitochondrial biogenesis during ageing in C. elegans. Nature *521*, 525-528.
41. Narendra, D.P., and Youle, R.J. (2011). Targeting mitochondrial dysfunction: role for PINK1 and Parkin in mitochondrial quality control. Antioxid Redox Signal *14*, 1929-1938.
42. Koopman, M., Michels, H., Dancy, B.M., Kamble, R., Mouchiroud, L., Auwerx, J., Nollen, E.A., and Houtkooper, R.H. (2016). A screening-based platform for the assessment of cellular respiration in Caenorhabditis elegans. Nat Protoc *11*, 1798-1816.
43. Schieke, S.M., Phillips, D., McCoy, J.P., Jr., Aponte, A.M., Shen, R.F., Balaban, R.S., and Finkel, T. (2006). The mammalian target of rapamycin (mTOR) pathway regulates mitochondrial oxygen consumption and oxidative capacity. J Biol Chem *281*, 27643-27652.
44. Van Raamsdonk, J.M., Meng, Y., Camp, D., Yang, W., Jia, X., Benard, C., and Hekimi, S. (2010). Decreased energy metabolism extends life span in Caenorhabditis elegans without reducing oxidative damage. Genetics *185*, 559-571.
45. Wang, M., Xue, Y., Shen, L., Qin, P., Sang, X., Tao, Z., Yi, J., Wang, J., Liu, P., and Cheng, H. (2019). Inhibition of SGK1 confers vulnerability to redox dysregulation in cervical cancer. Redox Biol *24*, 101225.
46. Jian, C., Xu, F., Hou, T., Sun, T., Li, J., Cheng, H., and Wang, X. (2017). Deficiency of PHB complex impairs respiratory supercomplex formation and activates mitochondrial flashes. J Cell Sci *130*, 2620-2630.
47. Schaar, C.E., Dues, D.J., Spielbauer, K.K., Machiela, E., Cooper, J.F., Senchuk, M., Hekimi, S., and Van Raamsdonk, J.M. (2015). Mitochondrial and cytoplasmic ROS have opposing effects on lifespan. PLoS Genet *11*, e1004972.
48. Yang, W., and Hekimi, S. (2010). A mitochondrial superoxide signal triggers increased longevity in Caenorhabditis elegans. PLoS Biol *8*, e1000556.
49. Van Raamsdonk, J.M., and Hekimi, S. (2009). Deletion of the mitochondrial superoxide dismutase sod-2 extends lifespan in Caenorhabditis elegans. PLoS Genet *5*, e1000361.
50. Ventura, N., Rea, S.L., and Testi, R. (2006). Long-lived C. elegans mitochondrial mutants as a model for human mitochondrial-associated diseases. Exp Gerontol *41*, 974-991.

1034 51. Senchuk, M.M., Dues, D.J., Schaar, C.E., Johnson, B.K., Madaj, Z.B., Bowman, M.J., Winn,
1035 M.E., and Van Raamsdonk, J.M. (2018). Activation of DAF-16/FOXO by reactive oxygen
1036 species contributes to longevity in long-lived mitochondrial mutants in Caenorhabditis
1037 elegans. PLoS Genet *14*, e1007268.
1038 52. Fang, E.F., Waltz, T.B., Kassahun, H., Lu, Q., Kerr, J.S., Morevati, M., Fivenson, E.M.,
1039 Wollman, B.N., Marosi, K., Wilson, M.A., et al. (2017). Tomatidine enhances lifespan and
1040 healthspan in C. elegans through mitophagy induction via the SKN-1/Nrf2 pathway. Sci Rep
1041 *7*, 46208.
1042 53. Kamal, M., D'Amora, D.R., and Kubiseski, T.J. (2016). Loss of hif-1 promotes resistance to
1043 the exogenous mitochondrial stressor ethidium bromide in Caenorhabditis elegans. BMC
1044 Cell Biol *17 Suppl 1*, 34.
1045 54. Hwang, A.B., Ryu, E.A., Artan, M., Chang, H.W., Kabir, M.H., Nam, H.J., Lee, D., Yang, J.S.,
1046 Kim, S., Mair, W.B., et al. (2014). Feedback regulation via AMPK and HIF-1 mediates ROS-
1047 dependent longevity in Caenorhabditis elegans. Proc Natl Acad Sci U S A *111*, E4458-4467.
1048 55. Lee, S.J., Hwang, A.B., and Kenyon, C. (2010). Inhibition of respiration extends C. elegans
1049 life span via reactive oxygen species that increase HIF-1 activity. Curr Biol *20*, 2131-2136.
1050 56. Mouchiroud, L., Houtkooper, R.H., Moullan, N., Katsyuba, E., Ryu, D., Canto, C., Mottis, A.,
1051 Jo, Y.S., Viswanathan, M., Schoonjans, K., et al. (2013). The NAD(+)/Sirtuin Pathway
1052 Modulates Longevity through Activation of Mitochondrial UPR and FOXO Signaling. Cell
1053 *154*, 430-441.
1054 57. Labbadia, J., Brielmann, R.M., Neto, M.F., Lin, Y.F., Haynes, C.M., and Morimoto, R.I.
1055 (2017). Mitochondrial Stress Restores the Heat Shock Response and Prevents Proteostasis
1056 Collapse during Aging. Cell Rep *21*, 1481-1494.
1057 58. Wu, Z., Senchuk, M.M., Dues, D.J., Johnson, B.K., Cooper, J.F., Lew, L., Machiela, E.,
1058 Schaar, C.E., DeJonge, H., Blackwell, T.K., et al. (2018). Mitochondrial unfolded protein
1059 response transcription factor ATFS-1 promotes longevity in a long-lived mitochondrial mutant
1060 through activation of stress response pathways. BMC Biol *16*, 147.
1061 59. Lev, I., Bril, R., Liu, Y., Cere, L.I., and Rechavi, O. (2019). Inter-generational consequences
1062 for growing Caenorhabditis elegans in liquid. Philos Trans R Soc Lond B Biol Sci *374*,
1063 20180125.
1064 60. Balklava, Z., Pant, S., Fares, H., and Grant, B.D. (2007). Genome-wide analysis identifies a
1065 general requirement for polarity proteins in endocytic traffic. Nat Cell Biol *9*, 1066-1073.
1066 61. Bomberger, J.M., Coutermarsh, B.A., Barnaby, R.L., Sato, J.D., Chapline, M.C., and
1067 Stanton, B.A. (2014). Serum and glucocorticoid-inducible kinase1 increases plasma
1068 membrane wt-CFTR in human airway epithelial cells by inhibiting its endocytic retrieval.
1069 PLoS One *9*, e89599.
1070 62. Zhu, M., Wu, G., Li, Y.X., Stevens, J.K., Fan, C.X., Spang, A., and Dong, M.Q. (2015).
1071 Serum- and Glucocorticoid-Inducible Kinase-1 (SGK-1) Plays a Role in Membrane
1072 Trafficking in Caenorhabditis elegans. PLoS One *10*, e0130778.
1073 63. deHart, A.K., Schnell, J.D., Allen, D.A., and Hicke, L. (2002). The conserved Pkh-Ypk kinase
1074 cascade is required for endocytosis in yeast. J Cell Biol *156*, 241-248.
1075 64. Bourgoint, C., Rispal, D., Berti, M., Filipuzzi, I., Helliwell, S.B., Prouteau, M., and Loewith, R.
1076 (2018). Target of rapamycin complex 2-dependent phosphorylation of the coat protein Pan1
1077 by Akl1 controls endocytosis dynamics in Saccharomyces cerevisiae. J Biol Chem *293*,
1078 12043-12053.
1079 65. Magner, D.B., Wollam, J., Shen, Y., Hoppe, C., Li, D., Latza, C., Rottiers, V., Hutter, H., and
1080 Antebi, A. (2013). The NHR-8 nuclear receptor regulates cholesterol and bile acid
1081 homeostasis in C. elegans. Cell Metab *18*, 212-224.
1082 66. Thondamal, M., Witting, M., Schmitt-Kopplin, P., and Aguilaniu, H. (2014). Steroid hormone
1083 signalling links reproduction to lifespan in dietary-restricted Caenorhabditis elegans. Nat
1084 Commun *5*, 4879.
1085 67. Chamoli, M., Singh, A., Malik, Y., and Mukhopadhyay, A. (2014). A novel kinase regulates
1086 dietary restriction-mediated longevity in Caenorhabditis elegans. Aging Cell *13*, 641-655.
1087 68. Brown, M.S., and Goldstein, J.L. (1997). The SREBP pathway: regulation of cholesterol
1088 metabolism by proteolysis of a membrane-bound transcription factor. Cell *89*, 331-340.
1089 69. Horton, J.D., Goldstein, J.L., and Brown, M.S. (2002). SREBPs: activators of the complete
1090 program of cholesterol and fatty acid synthesis in the liver. J Clin Invest *109*, 1125-1131.

1091 70. Walker, A.K., Jacobs, R.L., Watts, J.L., Rottiers, V., Jiang, K., Finnegan, D.M., Shioda, T.,
1092 Hansen, M., Yang, F., Niebergall, L.J., et al. (2011). A conserved SREBP-
1093 1/phosphatidylcholine feedback circuit regulates lipogenesis in metazoans. Cell *147*, 840-
1094 852.
1095 71. Hagiwara, A., Cornu, M., Cybulski, N., Polak, P., Betz, C., Trapani, F., Terracciano, L., Heim,
1096 M.H., Ruegg, M.A., and Hall, M.N. (2012). Hepatic mTORC2 activates glycolysis and
1097 lipogenesis through Akt, glucokinase, and SREBP1c. Cell Metab *15*, 725-738.
1098 72. Admasu, T.D., Chaithanya Batchu, K., Barardo, D., Ng, L.F., Lam, V.Y.M., Xiao, L.,
1099 Cazenave-Gassiot, A., Wenk, M.R., Tolwinski, N.S., and Gruber, J. (2018). Drug Synergy
1100 Slows Aging and Improves Healthspan through IGF and SREBP Lipid Signaling. Dev Cell
1101 *47*, 67-79 e65.
1102 73. Nomura, T., Horikawa, M., Shimamura, S., Hashimoto, T., and Sakamoto, K. (2010). Fat
1103 accumulation in Caenorhabditis elegans is mediated by SREBP homolog SBP-1. Genes Nutr
1104 *5*, 17-27.
1105 74. Roelants, F.M., Breslow, D.K., Muir, A., Weissman, J.S., and Thorner, J. (2011). Protein
1106 kinase Ypk1 phosphorylates regulatory proteins Orm1 and Orm2 to control sphingolipid
1107 homeostasis in Saccharomyces cerevisiae. Proc Natl Acad Sci U S A *108*, 19222-19227.
1108 75. Berchtold, D., Piccolis, M., Chiaruttini, N., Riezman, I., Riezman, H., Roux, A., Walther, T.C.,
1109 and Loewith, R. (2012). Plasma membrane stress induces relocalization of Slm proteins and
1110 activation of TORC2 to promote sphingolipid synthesis. Nat Cell Biol *14*, 542-547.
1111 76. Zhang, H., Abraham, N., Khan, L.A., Hall, D.H., Fleming, J.T., and Gobel, V. (2011).
1112 Apicobasal domain identities of expanding tubular membranes depend on glycosphingolipid
1113 biosynthesis. Nat Cell Biol *13*, 1189-1201.
1114 77. Marks, G.L., and Wood, D.O. (1992). Nucleotide sequence of the Rickettsia prowazekii greA
1115 homolog. Nucleic Acids Res *20*, 3785.
1116 78. Goldstein, J.L., DeBose-Boyd, R.A., and Brown, M.S. (2006). Protein sensors for membrane
1117 sterols. Cell *124*, 35-46.
1118 79. Perry, R.J., and Ridgway, N.D. (2005). Molecular mechanisms and regulation of ceramide
1119 transport. Biochim Biophys Acta *1734*, 220-234.
1120 80. Smulan, L.J., Ding, W., Freinkman, E., Gujja, S., Edwards, Y.J.K., and Walker, A.K. (2016).
1121 Cholesterol-Independent SREBP-1 Maturation Is Linked to ARF1 Inactivation. Cell Rep *16*,
1122 9-18.
1123 81. Kaczmarek, B., Verbavatz, J.M., and Jackson, C.L. (2017). GBF1 and Arf1 function in
1124 vesicular trafficking, lipid homoeostasis and organelle dynamics. Biol Cell *109*, 391-399.
1125 82. Ackema, K.B., Sauder, U., Solinger, J.A., and Spang, A. (2013). The ArfGEF GBF-1 Is
1126 Required for ER Structure, Secretion and Endocytic Transport in C. elegans. PLoS One *8*,
1127 e67076.
1128 83. Ackema, K.B., Hench, J., Bockler, S., Wang, S.C., Sauder, U., Mergentaler, H., Westermann,
1129 B., Bard, F., Frank, S., and Spang, A. (2014). The small GTPase Arf1 modulates
1130 mitochondrial morphology and function. EMBO J *33*, 2659-2675.
1131 84. Salo, V.T., and Ikonen, E. (2019). Moving out but keeping in touch: contacts between
1132 endoplasmic reticulum and lipid droplets. Curr Opin Cell Biol *57*, 64-70.
1133 85. Brodsky, J.L., and Fisher, E.A. (2008). The many intersecting pathways underlying
1134 apolipoprotein B secretion and degradation. Trends Endocrinol Metab *19*, 254-259.
1135 86. Yen, K., Le, T.T., Bansal, A., Narasimhan, S.D., Cheng, J.X., and Tissenbaum, H.A. (2010).
1136 A comparative study of fat storage quantitation in nematode Caenorhabditis elegans using
1137 label and label-free methods. PLoS One *5*.
1138 87. Wang, H., Jiang, X., Wu, J., Zhang, L., Huang, J., Zhang, Y., Zou, X., and Liang, B. (2016).
1139 Iron Overload Coordinately Promotes Ferritin Expression and Fat Accumulation in
1140 Caenorhabditis elegans. Genetics *203*, 241-253.
1141 88. Clarke, J., Dephoure, N., Horecka, I., Gygi, S., and Kellogg, D. (2017). A conserved signaling
1142 network monitors delivery of sphingolipids to the plasma membrane in budding yeast. Mol
1143 Biol Cell *28*, 2589-2599.
1144 89. Betz, C., Stracka, D., Prescianotto-Baschong, C., Frieden, M., Demaurex, N., and Hall, M.N.
1145 (2013). Feature Article: mTOR complex 2-Akt signaling at mitochondria-associated
1146 endoplasmic reticulum membranes (MAM) regulates mitochondrial physiology. Proc Natl
1147 Acad Sci U S A *110*, 12526-12534.

1148 90. Wei, Y., Liu, M., Li, X., Liu, J., and Li, H. (2018). Origin of the Autophagosome Membrane in
1149 Mammals. Biomed Res Int *2018*, 1012789.
1150 91. Ezcurra, M., Benedetto, A., Sornda, T., Gilliat, A.F., Au, C., Zhang, Q., van Schelt, S.,
1151 Petrache, A.L., Wang, H., de la Guardia, Y., et al. (2018). C. elegans Eats Its Own Intestine
1152 to Make Yolk Leading to Multiple Senescent Pathologies. Curr Biol *28*, 2544-2556 e2545.
1153 92. Singh, P.K., Singh, S., and Ganesh, S. (2013). Activation of serum/glucocorticoid-induced
1154 kinase 1 (SGK1) underlies increased glycogen levels, mTOR activation, and autophagy
1155 defects in Lafora disease. Mol Biol Cell *24*, 3776-3786.
1156 93. Andres-Mateos, E., Brinkmeier, H., Burks, T.N., Mejias, R., Files, D.C., Steinberger, M.,
1157 Soleimani, A., Marx, R., Simmers, J.L., Lin, B., et al. (2013). Activation of
1158 serum/glucocorticoid-induced kinase 1 (SGK1) is important to maintain skeletal muscle
1159 homeostasis and prevent atrophy. EMBO Mol Med *5*, 80-91.
1160 94. Gosai, S.J., Kwak, J.H., Luke, C.J., Long, O.S., King, D.E., Kovatch, K.J., Johnston, P.A.,
1161 Shun, T.Y., Lazo, J.S., Perlmutter, D.H., et al. (2010). Automated high-content live animal
1162 drug screening using C. elegans expressing the aggregation prone serpin alpha1-antitrypsin
1163 Z. PLoS One *5*, e15460.
1164 95. Toth, M.L., Sigmond, T., Borsos, E., Barna, J., Erdelyi, P., Takacs-Vellai, K., Orosz, L.,
1165 Kovacs, A.L., Csikos, G., Sass, M., et al. (2008). Longevity pathways converge on autophagy
1166 genes to regulate life span in Caenorhabditis elegans. Autophagy *4*, 330-338.
1167 96. Lapierre, L.R., De Magalhaes Filho, C.D., McQuary, P.R., Chu, C.C., Visvikis, O., Chang,
1168 J.T., Gelino, S., Ong, B., Davis, A.E., Irazoqui, J.E., et al. (2013). The TFEB orthologue HLH-
1169 30 regulates autophagy and modulates longevity in Caenorhabditis elegans. Nat Commun
1170 *4*, 2267.
1171 97. Settembre, C., Di Malta, C., Polito, V.A., Garcia Arencibia, M., Vetrini, F., Erdin, S., Erdin,
1172 S.U., Huynh, T., Medina, D., Colella, P., et al. (2011). TFEB links autophagy to lysosomal
1173 biogenesis. Science *332*, 1429-1433.
1174 98. Zhang, H., Chang, J.T., Guo, B., Hansen, M., Jia, K., Kovacs, A.L., Kumsta, C., Lapierre,
1175 L.R., Legouis, R., Lin, L., et al. (2015). Guidelines for monitoring autophagy in
1176 Caenorhabditis elegans. Autophagy *11*, 9-27.
1177 99. Kimura, S., Noda, T., and Yoshimori, T. (2007). Dissection of the autophagosome maturation
1178 process by a novel reporter protein, tandem fluorescent-tagged LC3. Autophagy *3*, 452-460.
1179 100. Chang, J.T., Kumsta, C., Hellman, A.B., Adams, L.M., and Hansen, M. (2017).
1180 Spatiotemporal regulation of autophagy during Caenorhabditis elegans aging. Elife *6*.
1181 101. Tian, Y., Garcia, G., Bian, Q., Steffen, K.K., Joe, L., Wolff, S., Meyer, B.J., and Dillin, A.
1182 (2016). Mitochondrial Stress Induces Chromatin Reorganization to Promote Longevity and
1183 UPR(mt). Cell *165*, 1197-1208.
1184 102. Schiavi, A., Torgovnick, A., Kell, A., Megalou, E., Castelein, N., Guccini, I., Marzocchella, L.,
1185 Gelino, S., Hansen, M., Malisan, F., et al. (2013). Autophagy induction extends lifespan and
1186 reduces lipid content in response to frataxin silencing in C. elegans. Exp Gerontol *48*, 191-
1187 201.
1188 103. Melendez, A., and Levine, B. (2009). Autophagy in C. elegans. WormBook, 1-26.
1189 104. Nargund, A.M., Fiorese, C.J., Pellegrino, M.W., Deng, P., and Haynes, C.M. (2015).
1190 Mitochondrial and nuclear accumulation of the transcription factor ATFS-1 promotes
1191 OXPHOS recovery during the UPR(mt). Mol Cell *58*, 123-133.
1192 105. Wilkinson, M.F. (2019). Genetic paradox explained by nonsense. Nature *568*, 179-180.
1193 106. Kim, S., and Sieburth, D. (2018). Sphingosine Kinase Activates the Mitochondrial Unfolded
1194 Protein Response and Is Targeted to Mitochondria by Stress. Cell Rep *24*, 2932-2945 e2934.
1195 107. Liu, Y., Samuel, B.S., Breen, P.C., and Ruvkun, G. (2014). Caenorhabditis elegans pathways
1196 that surveil and defend mitochondria. Nature *508*, 406-410.
1197 108. Krueger, B., Haerteis, S., Yang, L., Hartner, A., Rauh, R., Korbmacher, C., and Diakov, A.
1198 (2009). Cholesterol depletion of the plasma membrane prevents activation of the epithelial
1199 sodium channel (ENaC) by SGK1. Cell Physiol Biochem *24*, 605-618.
1200 109. Murley, A., Yamada, J., Niles, B.J., Toulmay, A., Prinz, W.A., Powers, T., and Nunnari, J.
1201 (2017). Sterol transporters at membrane contact sites regulate TORC1 and TORC2
1202 signaling. J Cell Biol *216*, 2679-2689.
1203 110. Wu, H., Carvalho, P., and Voeltz, G.K. (2018). Here, there, and everywhere: The importance
1204 of ER membrane contact sites. Science *361*.

111. Menuz, V., Howell, K.S., Gentina, S., Epstein, S., Riezman, I., Fornallaz-Mulhauser, M., Hengartner, M.O., Gomez, M., Riezman, H., and Martinou, J.C. (2009). Protection of C. elegans from anoxia by HYL-2 ceramide synthase. Science *324*, 381-384.
112. Mosbech, M.B., Kruse, R., Harvald, E.B., Olsen, A.S., Gallego, S.F., Hannibal-Bach, H.K., Ejsing, C.S., and Faergeman, N.J. (2013). Functional loss of two ceramide synthases elicits autophagy-dependent lifespan extension in C. elegans. PLoS One *8*, e70087.
113. Cutler, R.G., Thompson, K.W., Camandola, S., Mack, K.T., and Mattson, M.P. (2014). Sphingolipid metabolism regulates development and lifespan in Caenorhabditis elegans. Mech Ageing Dev *143-144*, 9-18.
114. Betz, C., and Hall, M.N. (2013). Where is mTOR and what is it doing there? J Cell Biol *203*, 563-574.
115. Csordas, G., Thomas, A.P., and Hajnoczky, G. (1999). Quasi-synaptic calcium signal transmission between endoplasmic reticulum and mitochondria. EMBO J *18*, 96-108.
116. Rizzuto, R., Pinton, P., Carrington, W., Fay, F.S., Fogarty, K.E., Lifshitz, L.M., Tuft, R.A., and Pozzan, T. (1998). Close contacts with the endoplasmic reticulum as determinants of mitochondrial Ca2+ responses. Science *280*, 1763-1766.
117. Stone, S.J., Levin, M.C., Zhou, P., Han, J., Walther, T.C., and Farese, R.V., Jr. (2009). The endoplasmic reticulum enzyme DGAT2 is found in mitochondria-associated membranes and has a mitochondrial targeting signal that promotes its association with mitochondria. J Biol Chem *284*, 5352-5361.
118. Vance, J.E. (1990). Phospholipid synthesis in a membrane fraction associated with mitochondria. J Biol Chem *265*, 7248-7256.
119. Fujimoto, M., Hayashi, T., and Su, T.P. (2012). The role of cholesterol in the association of endoplasmic reticulum membranes with mitochondria. Biochem Biophys Res Commun *417*, 635-639.
120. Raturi, A., and Simmen, T. (2013). Where the endoplasmic reticulum and the mitochondrion tie the knot: the mitochondria-associated membrane (MAM). Biochim Biophys Acta *1833*, 213-224.
121. Verfaillie, T., Rubio, N., Garg, A.D., Bultynck, G., Rizzuto, R., Decuypere, J.P., Piette, J., Linehan, C., Gupta, S., Samali, A., et al. (2012). PERK is required at the ER-mitochondrial contact sites to convey apoptosis after ROS-based ER stress. Cell Death Differ *19*, 1880-1891.
122. Hamasaki, M., Furuta, N., Matsuda, A., Nezu, A., Yamamoto, A., Fujita, N., Oomori, H., Noda, T., Haraguchi, T., Hiraoka, Y., et al. (2013). Autophagosomes form at ER-mitochondria contact sites. Nature *495*, 389-393.
123. Ardail, D., Popa, I., Bodennec, J., Louisot, P., Schmitt, D., and Portoukalian, J. (2003). The mitochondria-associated endoplasmic-reticulum subcompartment (MAM fraction) of rat liver contains highly active sphingolipid-specific glycosyltransferases. Biochem J *371*, 1013-1019.
124. Bionda, C., Portoukalian, J., Schmitt, D., Rodriguez-Lafrasse, C., and Ardail, D. (2004). Subcellular compartmentalization of ceramide metabolism: MAM (mitochondria-associated membrane) and/or mitochondria? Biochem J *382*, 527-533.
125. Birner, R., Nebauer, R., Schneiter, R., and Daum, G. (2003). Synthetic lethal interaction of the mitochondrial phosphatidylethanolamine biosynthetic machinery with the prohibitin complex of Saccharomyces cerevisiae. Mol Biol Cell *14*, 370-383.
126. Klecker, T., Wemmer, M., Haag, M., Weig, A., Bockler, S., Langer, T., Nunnari, J., and Westermann, B. (2015). Interaction of MDM33 with mitochondrial inner membrane homeostasis pathways in yeast. Sci Rep *5*, 18344.
127. Richter-Dennerlein, R., Korwitz, A., Haag, M., Tatsuta, T., Dargazanli, S., Baker, M., Decker, T., Lamkemeyer, T., Rugarli, E.I., and Langer, T. (2014). DNAJC19, a mitochondrial cochaperone associated with cardiomyopathy, forms a complex with prohibitins to regulate cardiolipin remodeling. Cell Metab *20*, 158-171.
128. van der Laan, M., Bohnert, M., Wiedemann, N., and Pfanner, N. (2012). Role of MINOS in mitochondrial membrane architecture and biogenesis. Trends Cell Biol *22*, 185-192.
129. Kornmann, B., Currie, E., Collins, S.R., Schuldiner, M., Nunnari, J., Weissman, J.S., and Walter, P. (2009). An ER-mitochondria tethering complex revealed by a synthetic biology screen. Science *325*, 477-481.
130. Strub, G.M., Paillard, M., Liang, J., Gomez, L., Allegood, J.C., Hait, N.C., Maceyka, M., Price, M.M., Chen, Q., Simpson, D.C., et al. (2011). Sphingosine-1-phosphate produced by

1263 sphingosine kinase 2 in mitochondria interacts with prohibitin 2 to regulate complex IV
1264 assembly and respiration. FASEB J *25*, 600-612.
1265 131. Brenner, S. (1974). The genetics of Caenorhabditis elegans. Genetics *77*, 71-94.
1266 132. Hall, D.H., Hartwieg, E., and Nguyen, K.C. (2012). Modern electron microscopy methods for
1267 C. elegans. Methods Cell Biol *107*, 93-149.
1268 133. Luz, A.L., Rooney, J.P., Kubik, L.L., Gonzalez, C.P., Song, D.H., and Meyer, J.N. (2015).
1269 Mitochondrial Morphology and Fundamental Parameters of the Mitochondrial Respiratory
1270 Chain Are Altered in Caenorhabditis elegans Strains Deficient in Mitochondrial Dynamics
1271 and Homeostasis Processes. PLoS One *10*, e0130940.
1272

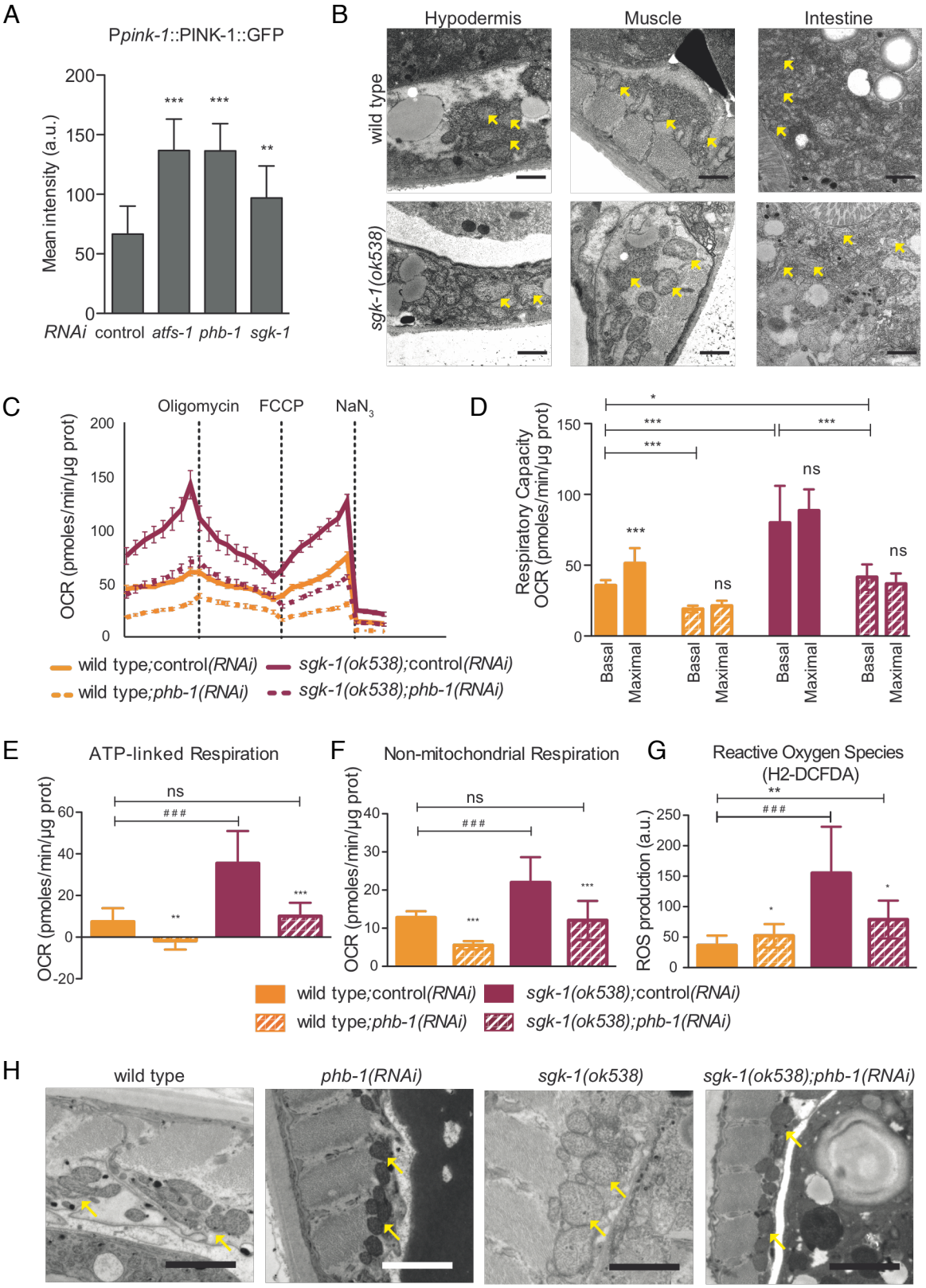

Figure 1: Altered mitochondrial structure and function of *sgk-1* mutants suppressed by prohibitin depletion. A. Quantification of P*pink-1*::PINK-1::GFP in worms treated with RNAi against *atfs-1*, *phb-1* and *sgk-1* at the young adult stage. **B.** Electron microscopy images of hypodermis, muscle and intestine of wild type and *sgk-1* mutants at day 1 of adulthood. Yellow arrows show mitochondria. Bar size: 1 µm. **C-F.** Seahorse measurements in wild type animals, *phb-1(RNAi)* treated worms, *sgk-1* mutants and *sgk-1;phb-1* depleted mutants at the young adult stage. **C.** Mitochondrial oxygen consumption rate. **D.** Basal and maximal respiratory capacity. **E.** ATP-linked respiration and **F.** Non-mitochondrial respiration. **G.** Reactive oxygen species (ROS) levels measured at the young adult stage of wild type animals, *phb-1(RNAi)* treated worms, *sgk-1* mutants and *sgk-1;phb-1* depleted mutants. **H.** Electron microscopy images of muscle cells, at day 5 of adulthood, of wild type and *sgk-1(ok538)* mutants under normal and mitochondrial stress conditions (*phb-1(RNAi)*). Yellow arrows point to mitochondria. Bar size: 1 µm. (Mean ± SD; *** p value < 0.001, ** p value < 0.01, * p value < 0.1, ns not significant compared against its respective *control(RNAi)*, ### p value < 0.001 compared against wild type *control(RNAi)*; *t-test*. Combination of three independent replicates).

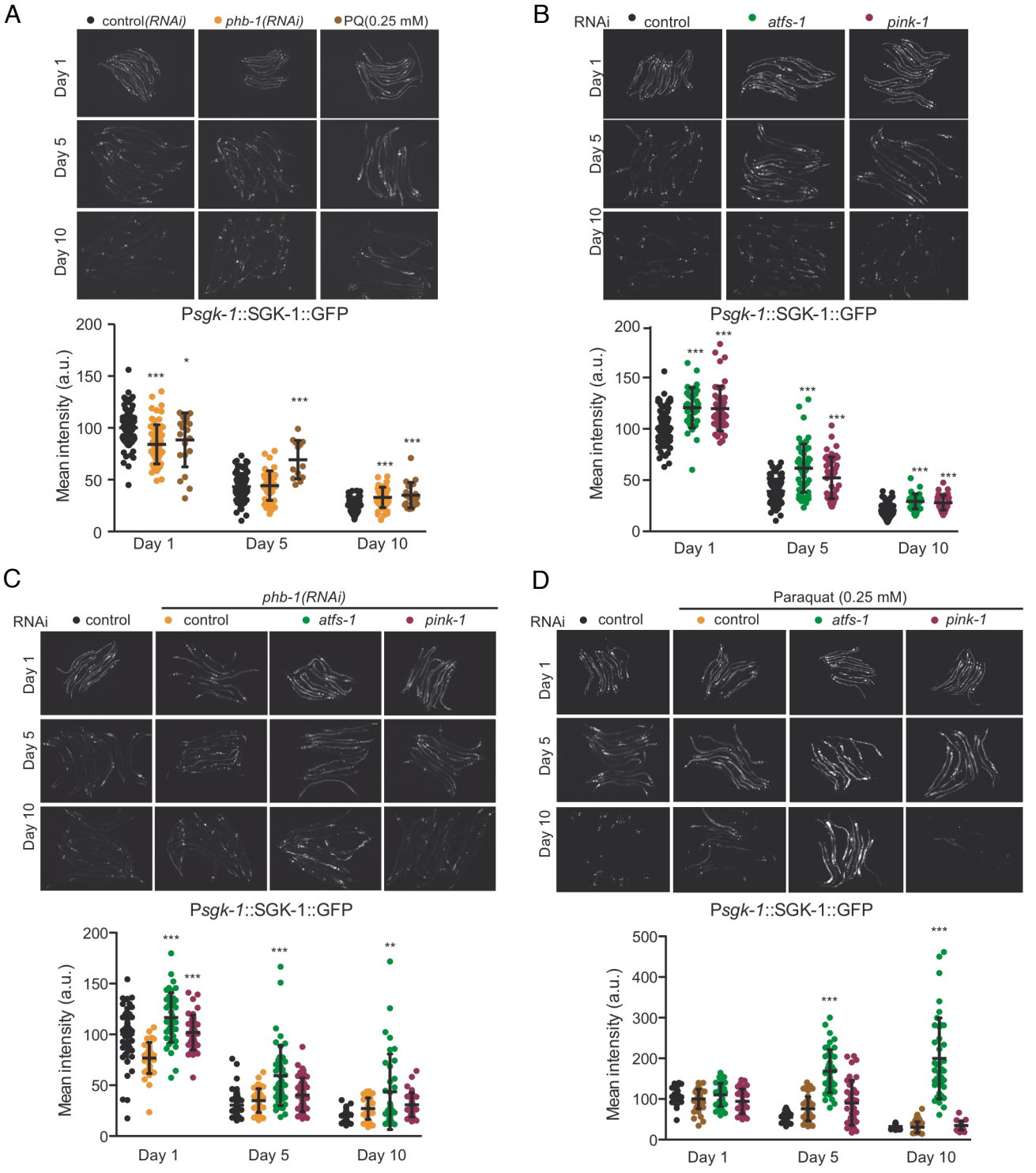

Figure 2: SGK-1 protein levels differentially respond to mitochondrial quality control mechanisms, depending on the level of mitochondrial stress. A. SGK-1 protein levels during aging, from day 1 to day 10 upon strong mitochondrial stress caused by PHB depletion or treating worms with Paraquat (PQ) (0.25 mM). **B.** SGK-1 protein levels at day 1, day 5 and day 10 upon inhibition of mitochondrial quality control mechanisms; UPR^{mt} by *atfs-1(RNAi)* and mitophagy by *pink-1(RNAi)*. **C.** SGK-1 protein levels at day 1, day 5 and day 10 upon combination of mitochondrial stress by PHB depletion and inhibition of either the UPR^{mt} (*atfs-1(RNAi)*) or mitophagy (*pink-1(RNAi)*). **D.** SGK-1 protein levels at day 1, day 5 and day 10 upon combination of mitochondrial stress by PQ treatment and inhibition of either the UPR^{mt} (*atfs-1(RNAi)*) or mitophagy (*pink-1(RNAi)*) (Mean ± SD; *** p value < 0.001, ** p value < 0.01, * p value < 0.1, ns not significant; ANOVA test. Combination of at least three independent replicates.).

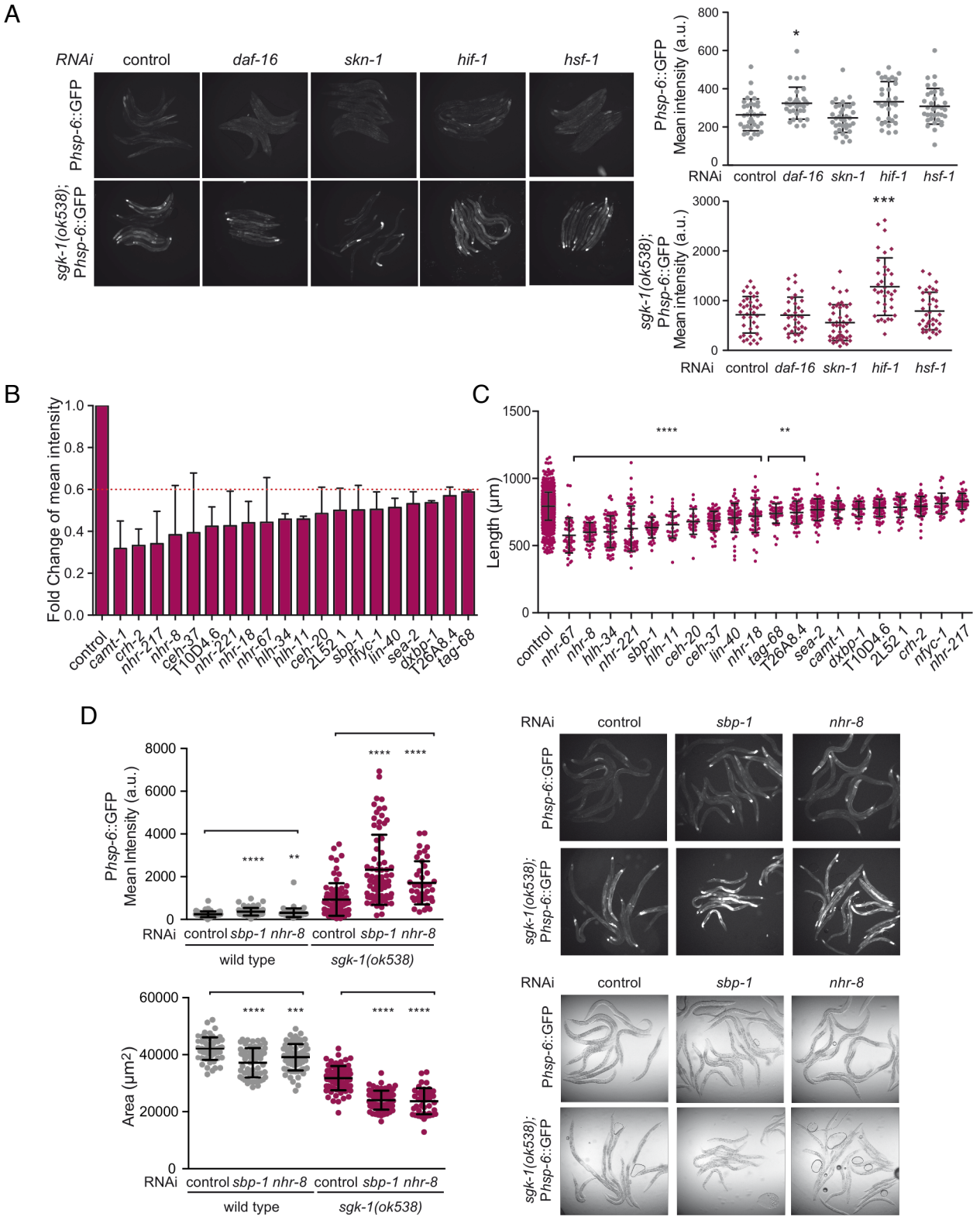

Figure 3: The UPR^{mt} in *sgk-1* mutants is modulated by a battery of transcription factors involved in membrane sterol and lipid homeostasis. A. Quantification of the UPR^{mt} reporter P*hsp-6*::GFP in wild type animals (left) and *sgk-1* mutants (right) upon depletion of *daf-16, skn-1, hif-1* and *hsf-1*. (Mean ± SD; *** *p* value < 0.001, * *p* value < 0.1 compared against control(RNAi); ANOVA test). Representative images are shown. **B.** Fold change of GFP intensity of the 20 clones whose depletion reduces the mitochondrial stress response in *sgk-1* mutants.C**.** Length of the worms (µm) upon depletion of the 20 candidates in *sgk-1* mutants. **D.** Quantification of the UPR^{mt} reporter (left upper panel) and worm area (left bottom panel) in wild type animals and *sgk-1* mutants upon depletion of *sbp-1* and *nhr-8* (Mean ± SD; **** *p* value < 0.0001, *** *p* value < 0.001, ** *p* value < 0.005 compared against control(RNAi); *t*-test). Representative images of the expression level of the UPR^{mt} reporter are shown in the right upper panel, brightfield images in the right bottom panel.

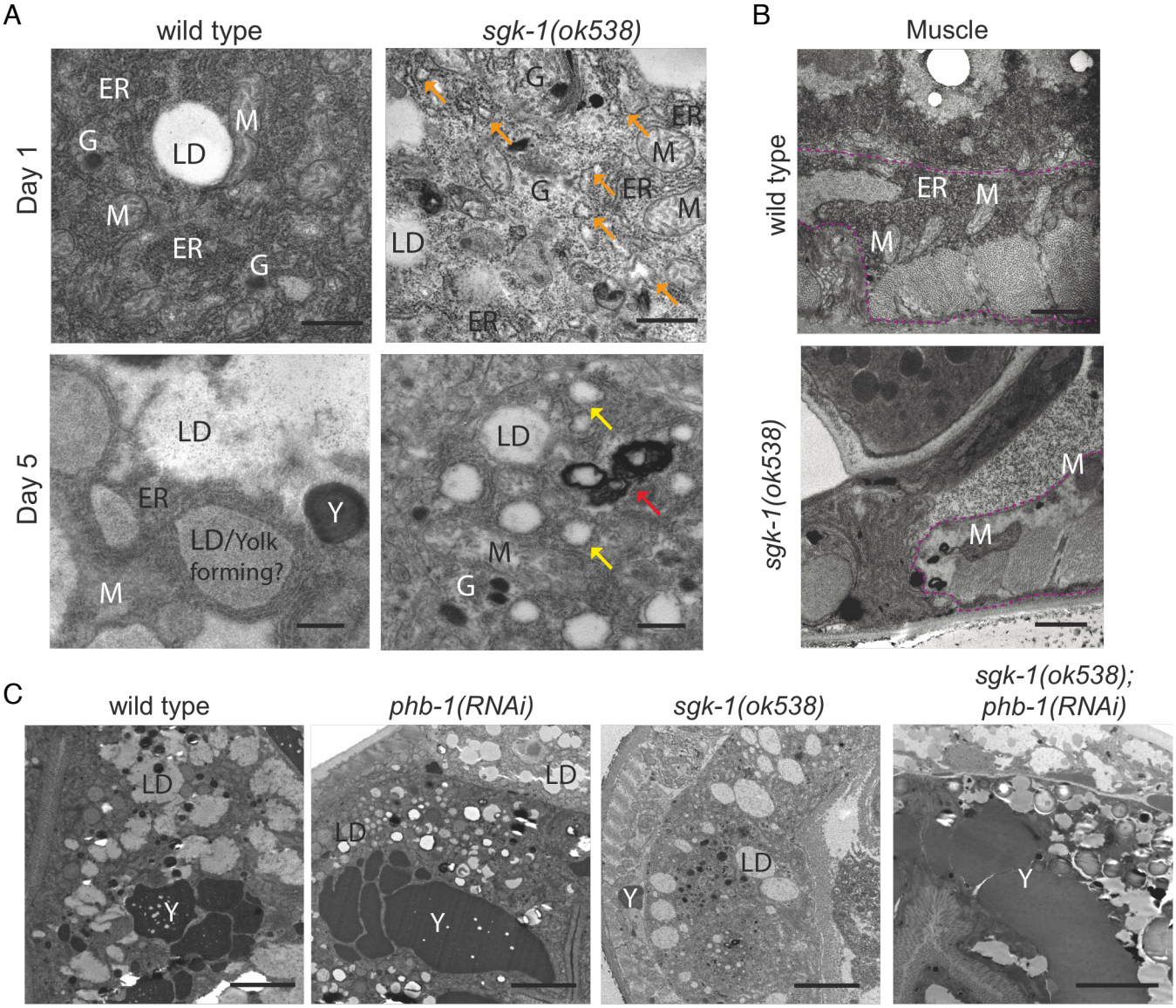

Figure 4: Impaired lipogenesis and lipoprotein/yolk formation in *sgk-1* mutants is suppressed by prohibitin depletion

A. Transmission electron microscopy images of the first intestinal cells of wild type and *sgk-1* mutants during aging (day 1 and day 5 of adulthood). Orange arrows point to defective ER exit sites. Yellow arrows point to forming LD. Red arrow, point to abnormal autolysosomes/myelinated forms. Bar size: 500 nm. For more details see Supplementary figure S6. **B.** Transmission electron microscopy images of muscle, delineated with a purple dashed line, of wild type and *sgk-1* mutants at day 1 of adulthood. Bar size: 1 µm. **C.** Transmission electron microscopy images of wild type worms, *phb-1(RNAi)* treated worms, *sgk-1* mutants and *sgk-1;phb-1(RNAi)* treated mutants at day 5 of adulthood. Bar size: 5 µm. M: mitochondria, ER: Endoplasmic Reticulum, LD: Lipid Droplet, Y: Yolk, G: Golgi.

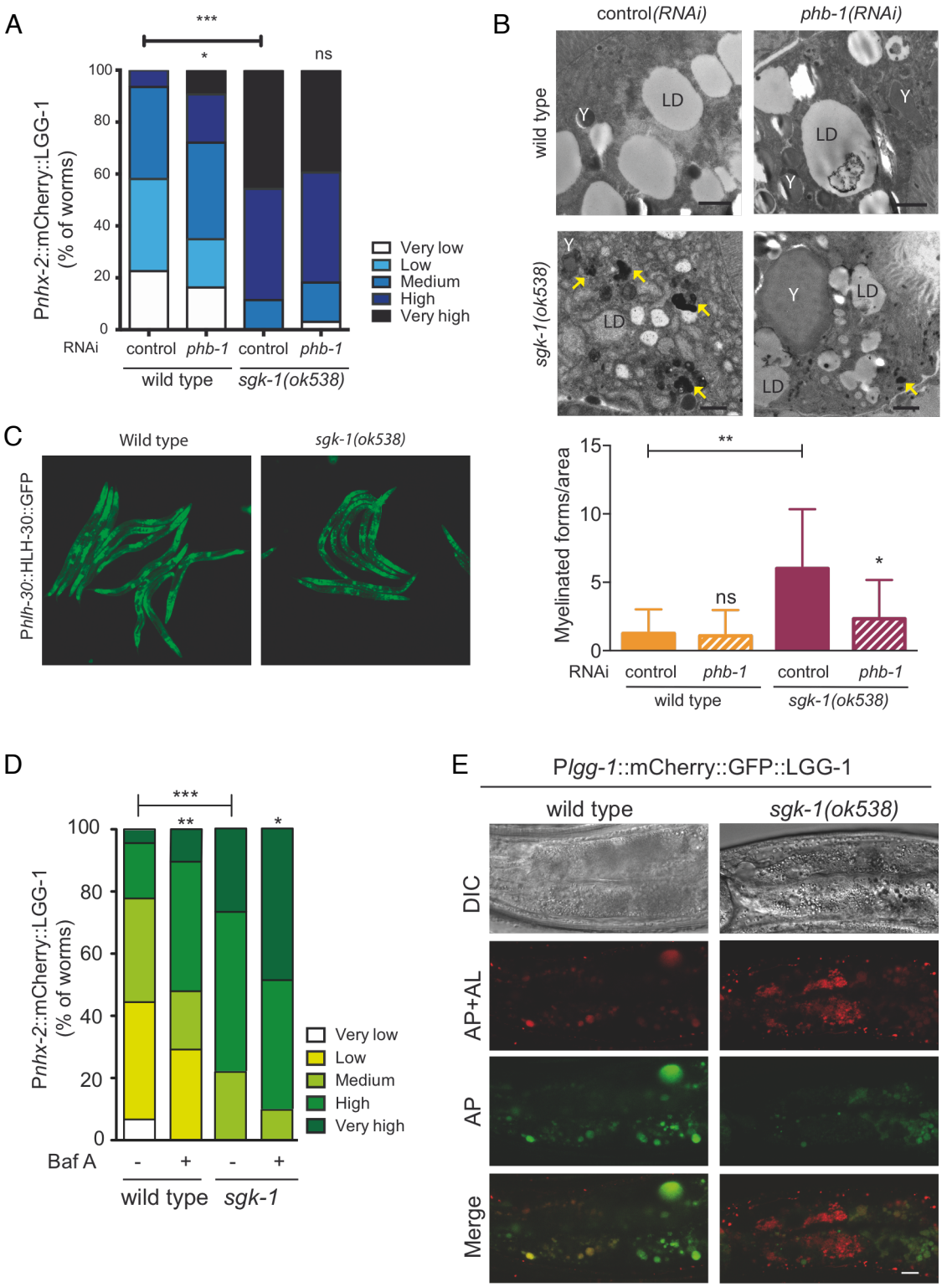

Figure 5: Impaired autophagy flux in *sgk-1* mutants is suppressed by prohibitin depletion. A. Quantification of the expression of the intestinal autophagy reporter Ex[P*nxh-2*::mCherry::LGG-1] (see materials and methods and figure S10) in wild type animals, *phb-1* depleted worms, *sgk-1* mutants and *sgk-1;phb-1(RNAi)* treated mutants at day 5 of adulthood. **B.** Electron microscopy images of wild type and *sgk-1* mutants in the intestine under basal and mitochondrial stress conditions (*phb-1(RNAi)*) at day 1 of adulthood. Yellow arrows show the myelinated forms that are quantified in the bottom panel. LD: lipid droplet, Y: yolk particles. Bar size: 1µm. **C.** Images of the reporter P*hlh-30*::HLH-30::GFP in wild type and *sgk-1* mutants at day 1 of adulthood in OP50. **D.** Quantification of the intestinal autophagy reporter Ex[P*nxh-2*::mCherry::LGG-1] in wild type animals and *sgk-1* mutants, treated or not with bafilomycin A1 (Baf A), at day 5 of adulthood in HT115. **E.** Images of the reporter P*lgg-1*::mCherry::GFP::LGG-1 in wild type animals and *sgk-1* mutants at day 5 of adulthood in OP50. Brightfield images are shown in the upper panel, red images correspond to autophagosomes (AP) and autolysosomes (AL) and green images correspond only to autophagosomes. Bottom panel show merged images. Bar size: 10 µm. (Mean ± SD; *** p value < 0.001,** p value < 0.01, * p value < 0.1, ns not significant; t-test. Combination of three independent replicates).

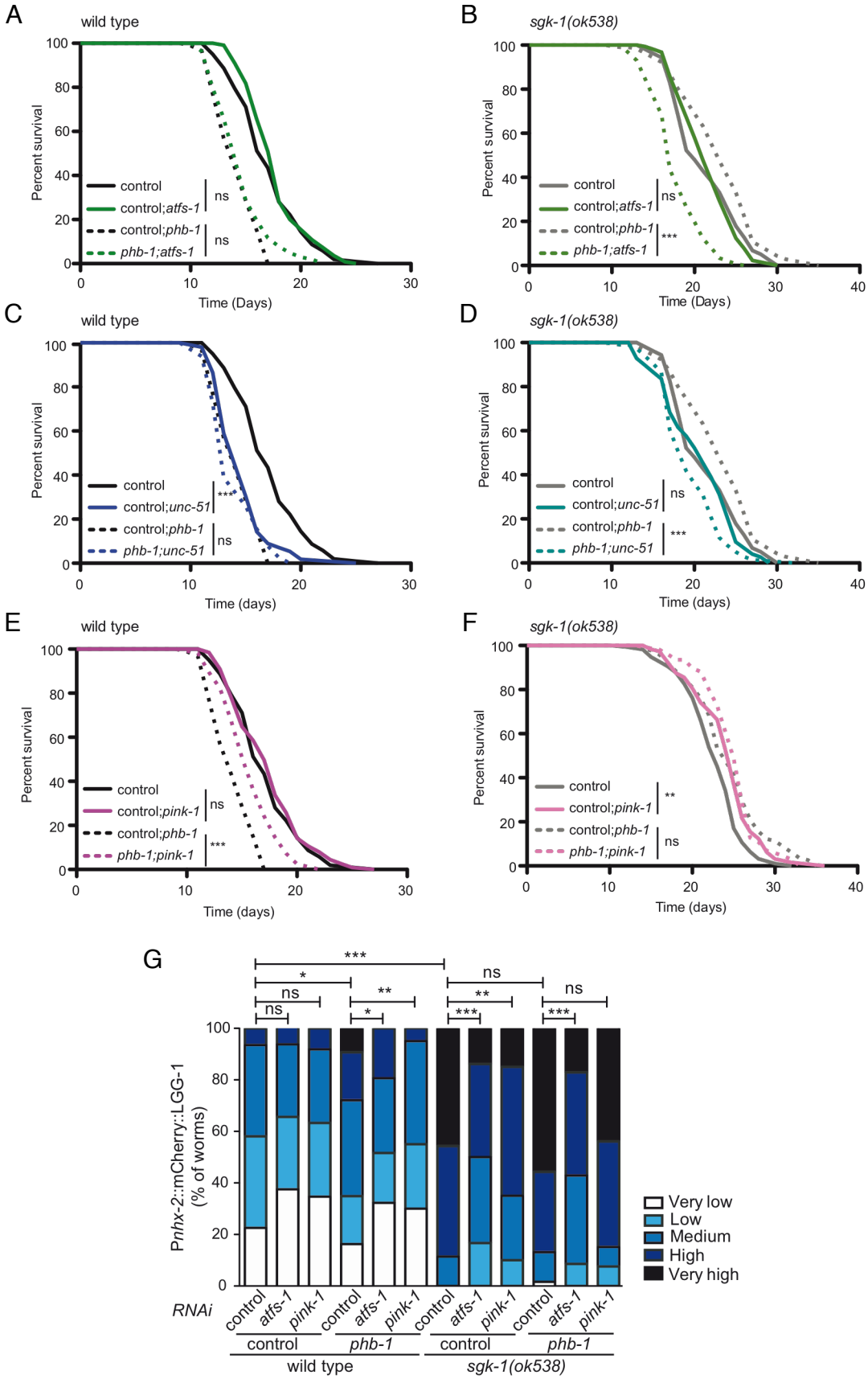

Figure 6: Autophagy and the UPR^{mt}, but not mitophagy, are required for the enhanced longevity of *sgk-1* mutants upon PHB depletion. Lifespan of wild type worms (left) and *sgk-1* mutants (right) under normal and mitochondrial stress conditions (*phb-1(RNAi)*) upon inhibition of the UPR^{mt} (**A** and **B**), inhibition of autophagy (**C** and **D**) and inhibition of mitophagy (**E** and **F**). One representative replicate is shown. Replicates and statistics are shown in table S1. **G.** Quantification of the autophagy reporter Ex[P*nxh-2*::mCherry::LGG-1] in wild type animals, *phb-1(RNAi)* treated worms, *sgk-1(ok538)* mutants and *sgk-1;phb-1 depleted* mutants at day 5 of adulthood upon inhibition of the UPR^{mt} (*atfs-1(RNAi)*) and inhibition of mitophagy (*pink-1(RNAi)*) (*** p value < 0.001, ** p value < 0.01, * p value < 0.1, ns not significant; t-test. Combination of at least three independent replicates).

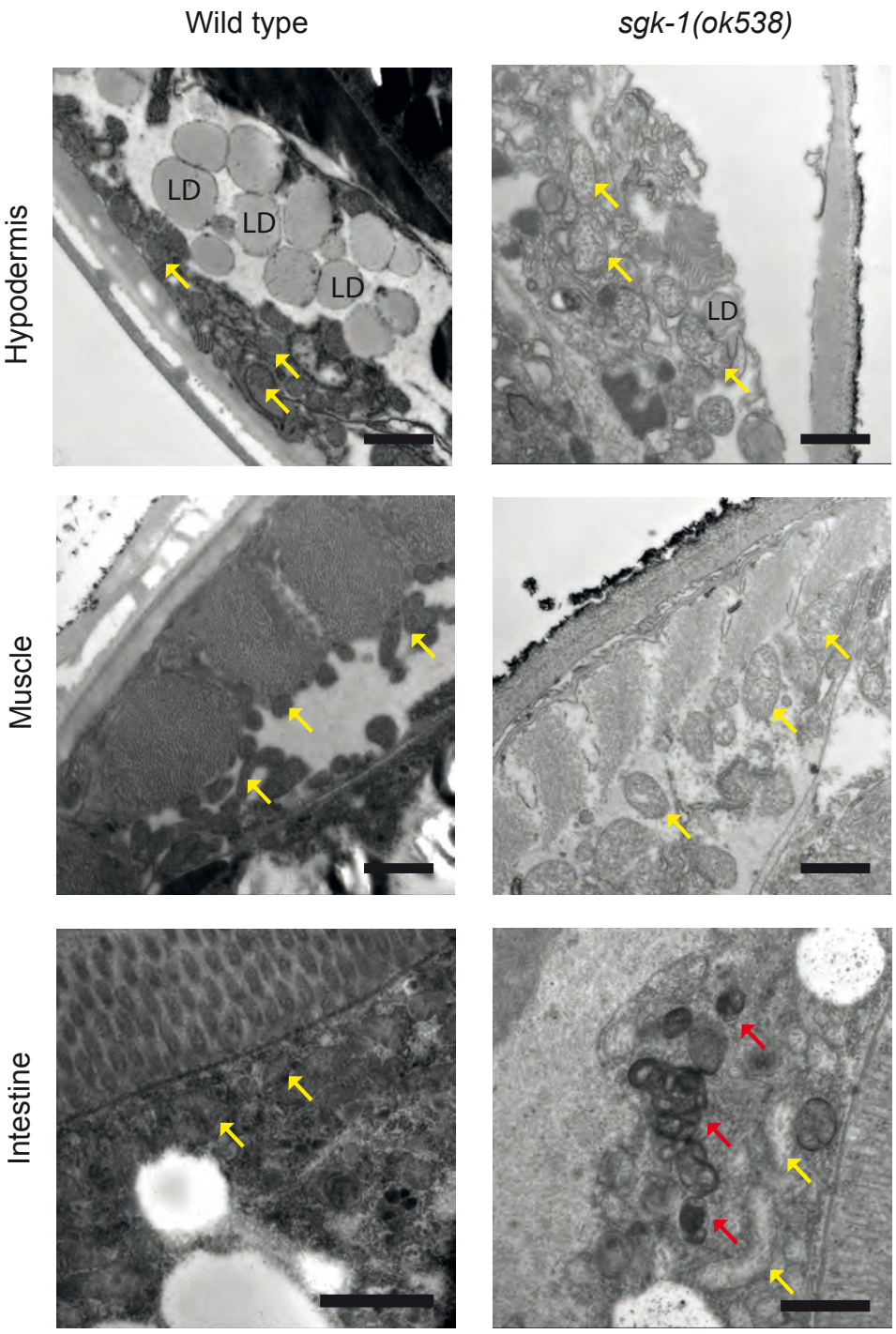

Figure S1: Electron microscopy images of hypodermal, muscle and intestinal tissue of wild type and *sgk-1(ok538)* mutants at day 5 of adulthood in HT115 bacteria. Yellow arrows point to mitochondria. Abnormal and swollen mitochondria can be observed in *sgk-1* mutants compared to wild type. Lipid droplets (LD) are labelled in the hypodermal tissue. In the intestine, abnormal autophagosomes, red arrows, are seen in *sgk-1* mutants. Bar size: 1µm.

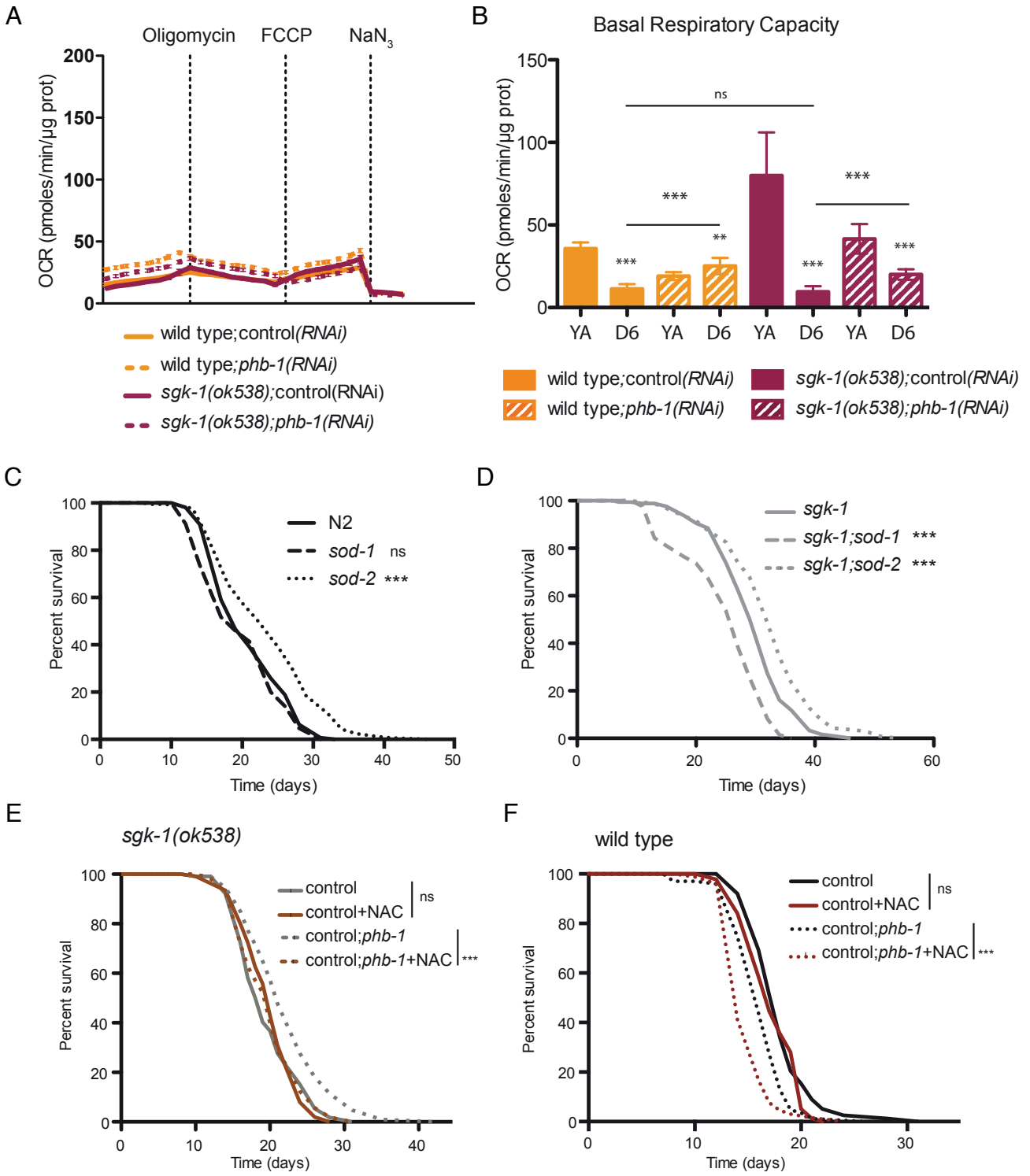

Figure S2: Oxygen consumption rate of wild type, *phb-1* depleted worms, *sgk-1* mutants and *sgk-1;phb-1(RNAi)* treated mutants at day 6 and lifespan of wild type and *sgk-1* mutants. A. Mitochondrial performance of wild type, *phb-1* depleted worms, *sgk-1* mutants and *sgk-1;phb-1(RNAi)* treated mutants at day 6 of adulthood. **B.** Basal respiratory capacity of wild type, *phb-1* depleted worms, *sgk-1* mutants and *sgk-1;phb-1(RNAi)* treated mutants at day 6 of adulthood. (Mean ± SD; *** p value < 0.001, ** p value < 0.01, ns not significant; t-test. Combination of three independent replicates is shown.). **C.** Lifespan of wild type, *sod-1* mutants and *sod-2* mutants. **D.** Lifespan of *sgk-1* mutants, *sgk-1;sod-1* and *sgk-1;sod-2* double mutants. Depletion of *sod-1* shortens lifespan of *sgk-1* mutants. **E.** Lifespan of *sgk-1* mutants and *sgk-1;phb-1(RNAi)* treated mutants upon treatment with the antioxidant NAC. NAC prevents the enhancement of *sgk-1* lifespan upon PHB depletion without affecting lifespan of *sgk-1* mutants. **F.** Lifespan of wild type worms and *phb-1* depleted worms upon treatment with the antioxidant NAC. Lifespan replicates and statistics are shown in table S1.

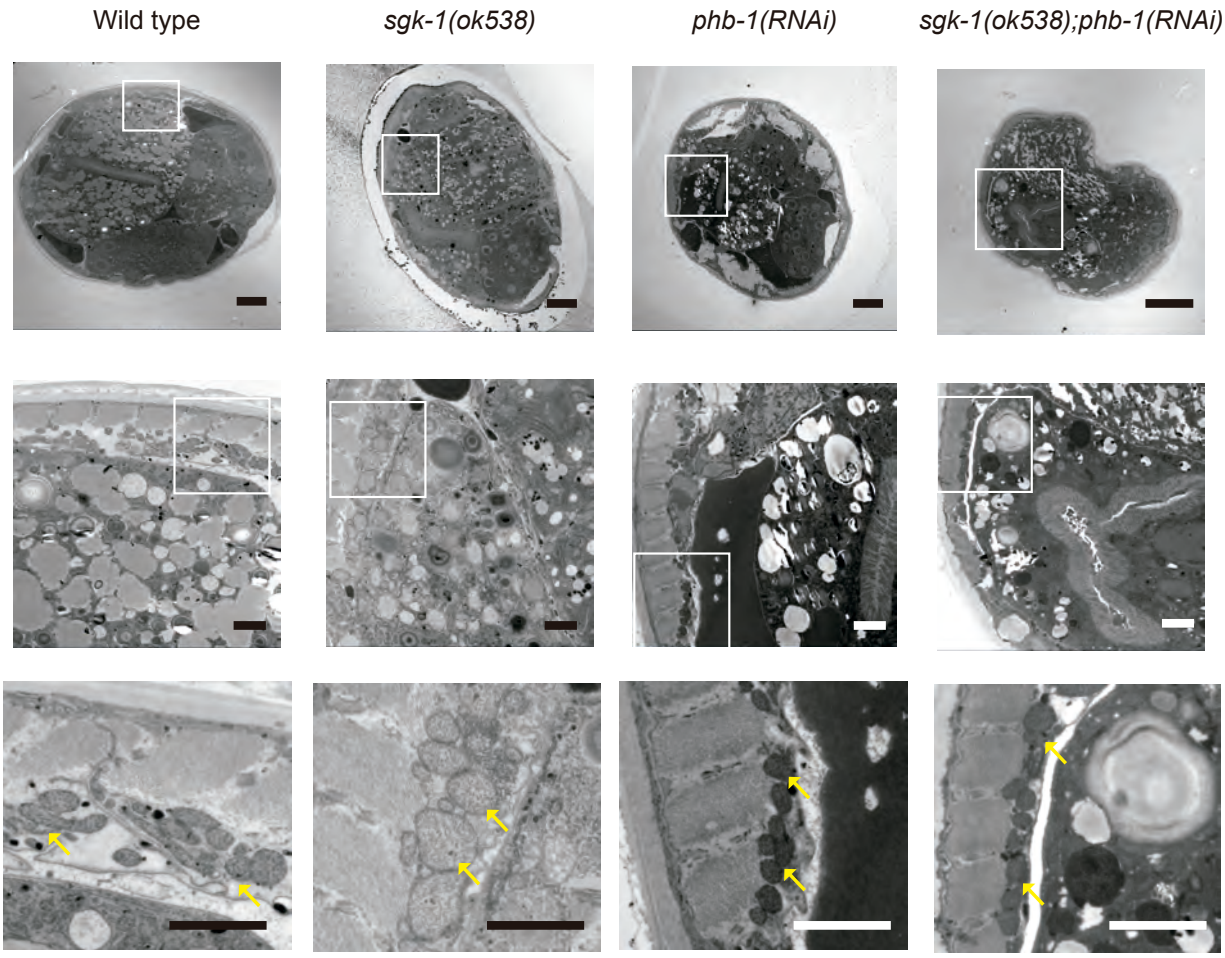

Figure S3: Electron microscopy images of muscle mitochondria of wild type, *sgk-1(ok538)* mutants, *phb-1(RNAi)* treated animals and *sgk-1(ok538)* mutants upon *phb-1(RNAi)* .Top images show a general view of a section. White boxes are magnified in the immediate image below. Yellow arrows point to mitochondria. Abnormal and swollen mitochondria can be observed in *sgk-1* mutants compared to wild type. Depletion of *phb-1* results in mitochondrial fragmentation in wild type worms and suppression of the increased mitochondrial size in *sgk-1* mutants. Bar sizes: 10 µm (top panel), 2 µm (middle and bottom panels).

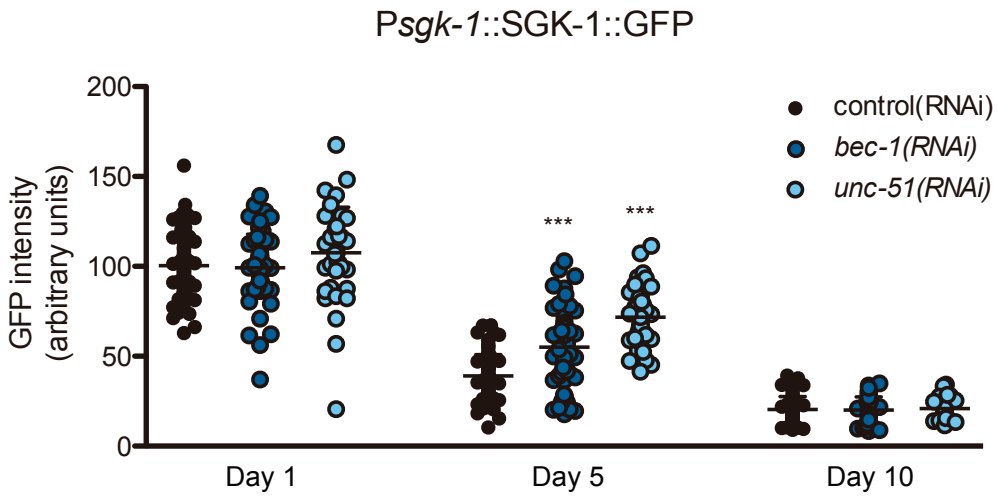

Figure S4: Ex[P*sgk-1*::SGK-1::GFP] expression levels at day 1, day 5 and day 10 of adulthood in animals treated with control(RNAi), *bec-1(RNAi)* and *unc-51(RNAi).* SGK-1 protein levels at day 1, day 5 and day 10 upon inhibition of different steps of autophagy: initiation (*unc-51(RNAi)*) and nucleation (*bec-1(RNAi)*). (Mean ± SD; *** p value < 0.001, ANOVA test. Combination of at least three independent replicates is shown.).

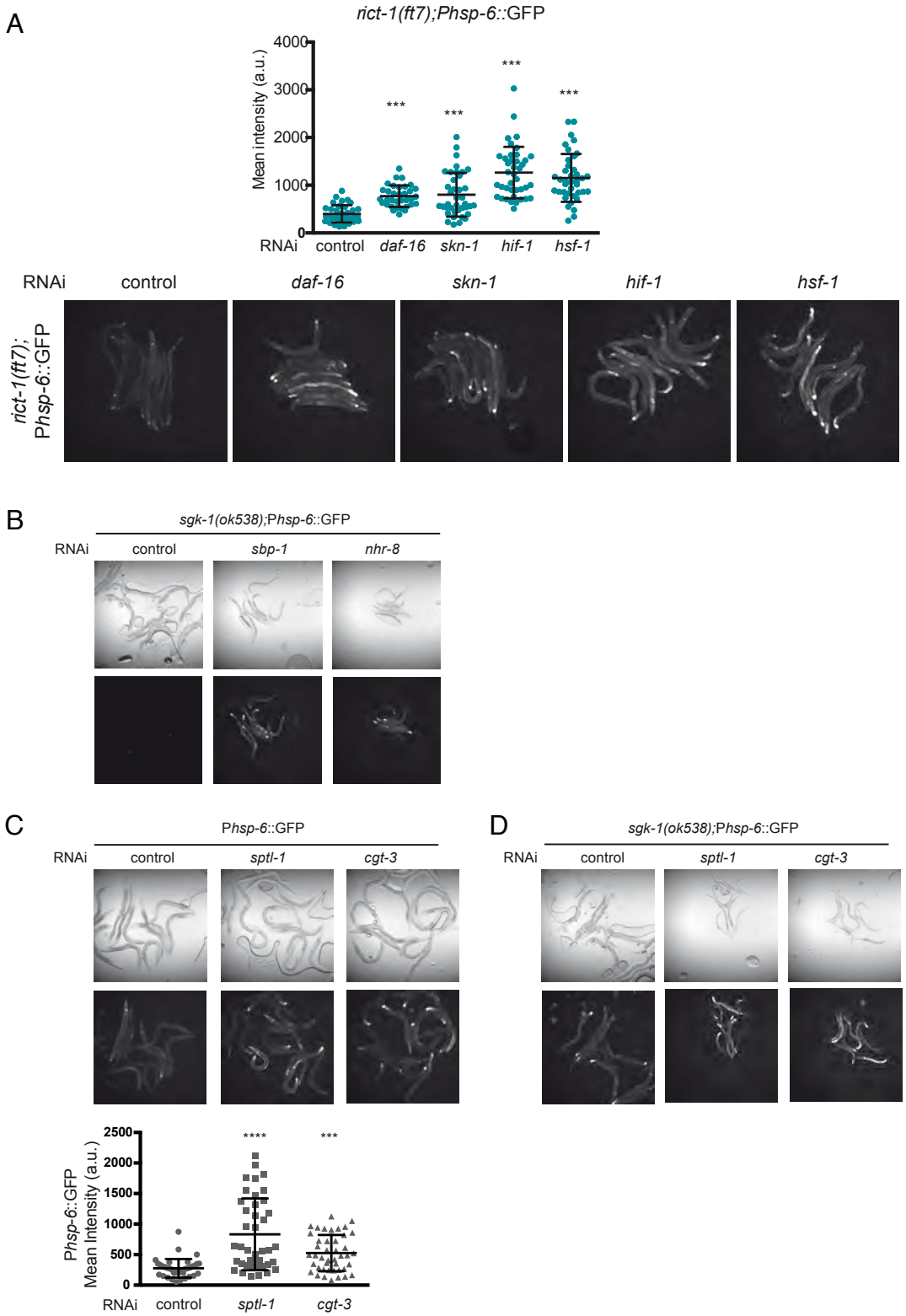

Figure S5: Quantification of the UPR^{mt} in *rict-1* mutants and effect of depleting lipid homeostasis genes on the UPR^{mt} in wild type and in *sgk-1* mutants. A. Quantification of the UPR^{mt} reporter in *ric-1* mutants upon depletion of *daf-16, skn-1, hif-1* and *hsf-1*. (Mean ± SD; *** p value < 0.001 compared against control(RNAi); ANOVA test). Representative images are shown. **B.** Developmental delay of *sgk-1* mutants upon depletion of *sbp-1* and *nhr-8*. Worms were imaged when *sgk-1* mutants reached the young adult stage. Induced UPR^{mt} upon depletion of *sbp-1* and *nhr-8* can be observed. **C.** Quantification of the UPR^{mt} reporter upon depletion of ceramide/sphingolipid genes *sptl-1* and *cgt-3* (Mean ± SD; **** p value < 0.0001, *** p value < 0.001; ANOVA test). Representative images are shown. **D.** Genetic interaction of *sgk-1* mutants with ceramide/sphingolipid genes *sptl-1* and *cgt-3*. Worms were imaged when *sgk-1* mutants reached the young adult stage. While *cgt-3* depleted animals eventually reached adulthood, *sptl-1* depletion arrested development of *sgk-1* mutants at the L3-L4 stage. Induced UPR^{mt} upon depletion of *sptl-1* and *cgt-3* can be observed.

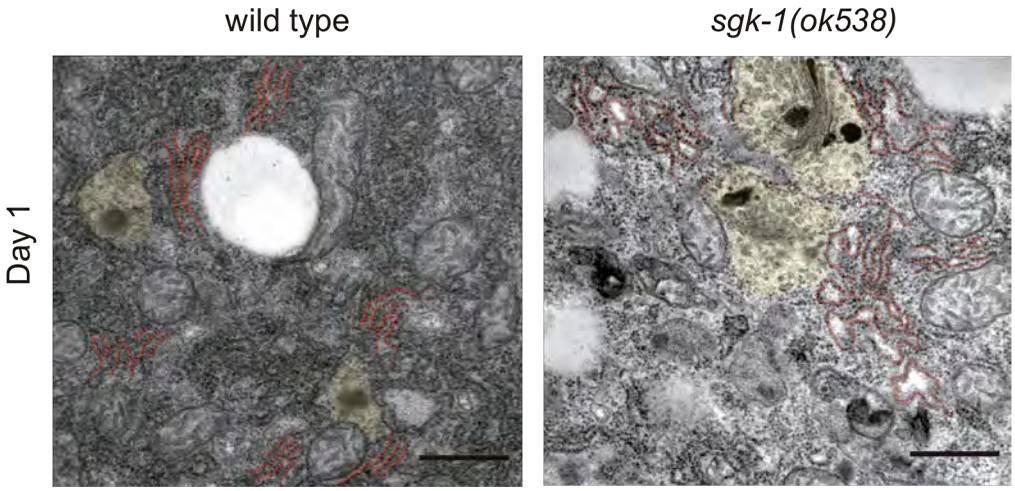

Figure S6: Electron microscopy images showing altered ER and Golgi dynamics. Transmission electron microscopy images of the first intestinal cells of wild type and *sgk-1* mutants at day 1, corresponding to figure 4a. Some endoplasmic reticulum is delineated with dashed red lines. Golgi apparatus and vesicles areas are highlighted with yellow shadows. Bar size: 500 nm.

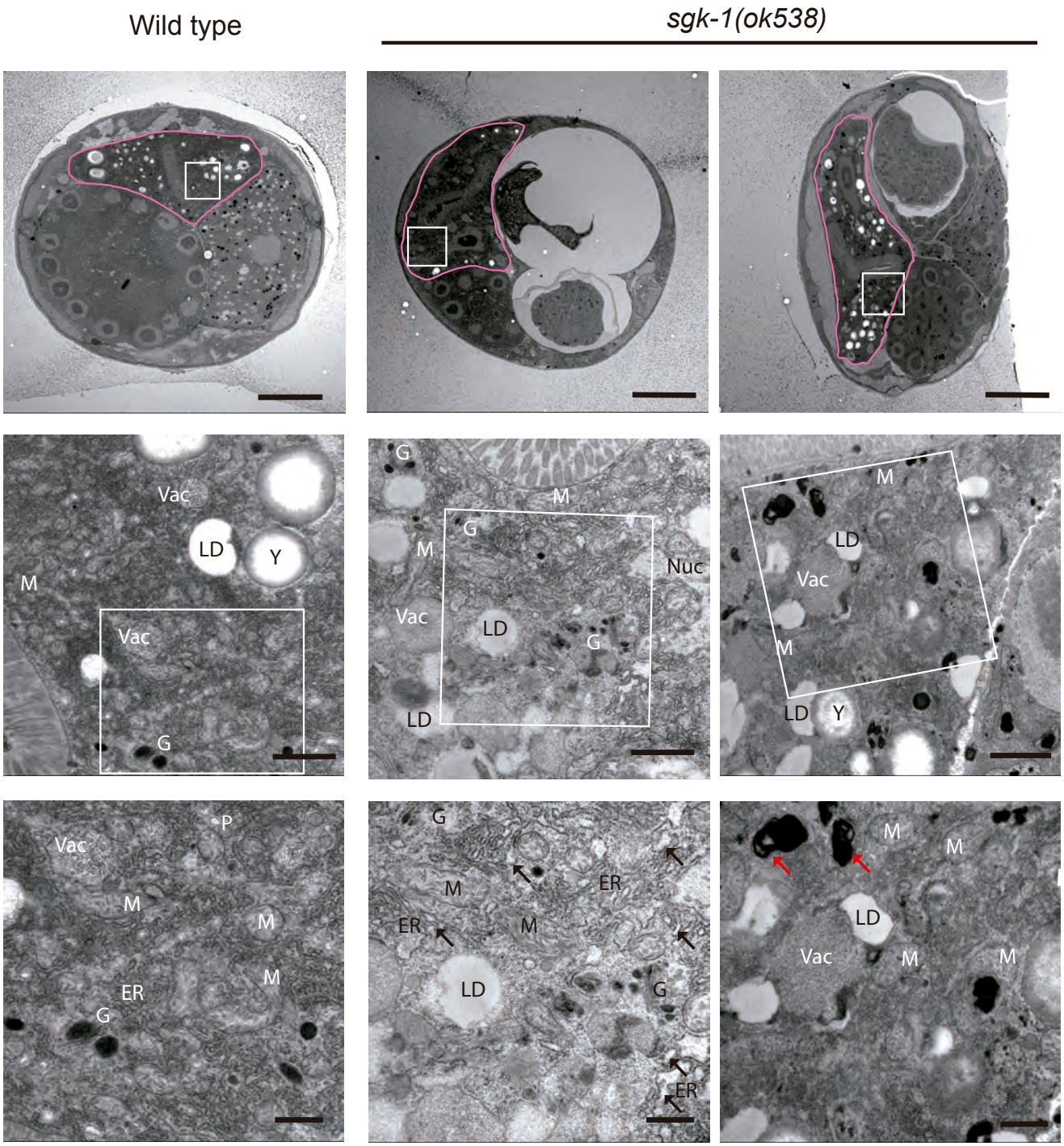

Figure S7: Electron microscopy images of the anterior intestinal cells of a wild-type and two *sgk-1(ok538)* adults grown in HT115 bacteria at day 1 of adulthood. Top images show a general view of a section where the intestine is delineated with a pink line. Membrane detachment of gonadal tissue can be observed in *sgk*-1 mutants. White squares are magnified in the immediate image below. M: mitochondria, LD: Lipid Droplets, ER: Endoplasmic Reticulum, G: Golgi, Y: Yolk, Vac: Vacuoles, Nuc: nucleus. Increased ER emanating structures (black arrows, bottom middle panel) and complex myelinated autophagic structures (red arrows, bottom right panel) are observed in *sgk-1* mutants. Bar sizes: 10 µm (top panels), 1 µm (middle panels) and 500 nm (bottom panels).

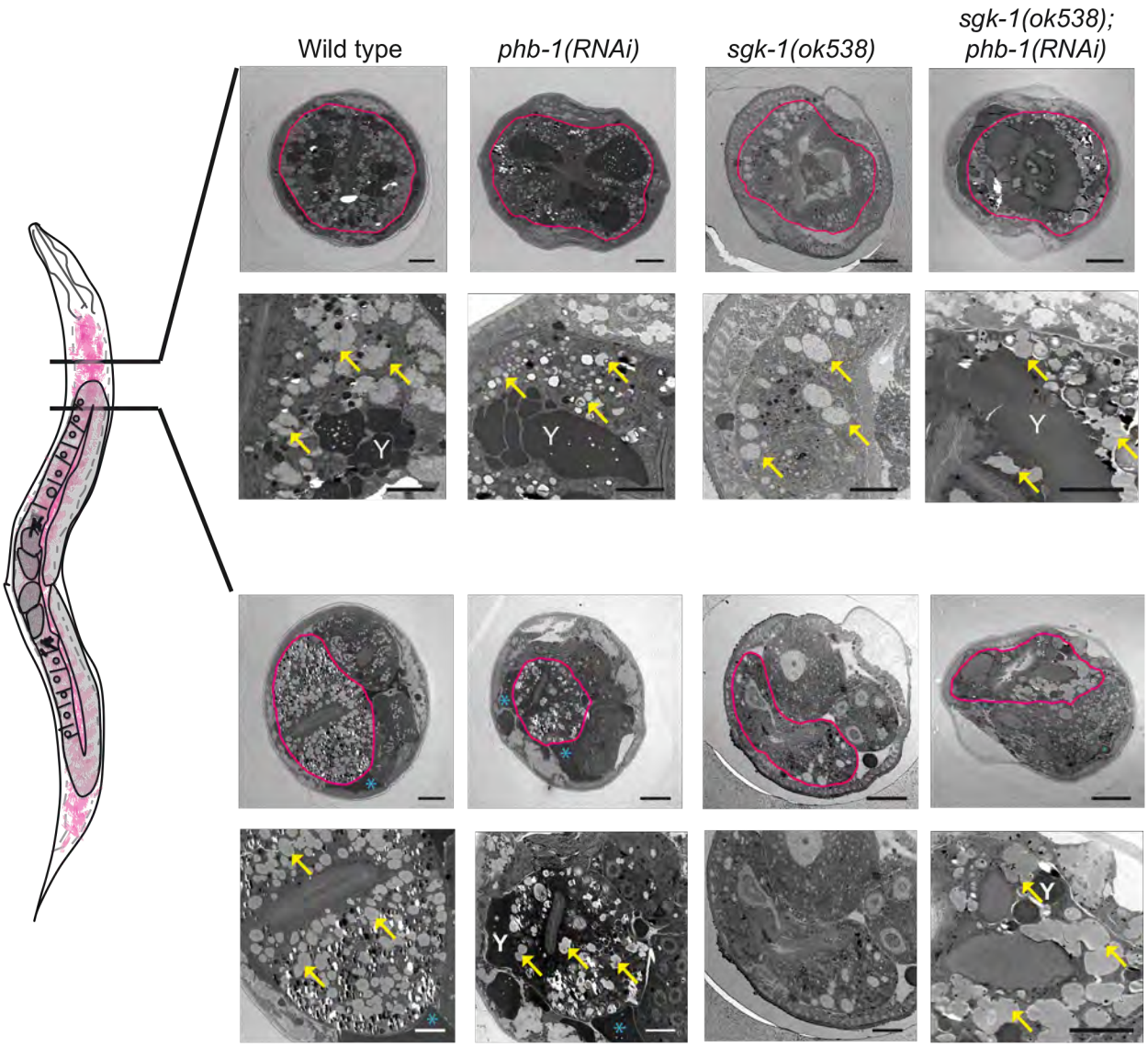

Figure S8: Electron microscopy images of the beginning of the intestine, before and after the gonad turn, of wild-type, *sgk-1* mutants, *phb-1* depleted animals and *sgk-1;phb-1(RNAi) treated* mutants at day 5 of adulthood.Top images show a general view of a section where the intestine is delineated with a pink line. Bottom images show a magnification where we observed that *sgk-1* mutants are defective in lipid droplet formation and vitellogenesis and have little accumulation of pseudocoelomic lipoproteins compared to wild type and prohibitin depleted animals. Depletion of the mitochondrial PHB complex suppressed both, lipid droplet accumulation and yolk production defects of *sgk-1* mutants. Bar sizes: 10 µm (top panels) and 5 µm (bottom panels) for each of the cuts. Intestinal yolk/lipoproteins are marked with Y, blue asterisks mark pseudocoelomic lipoproteins and yellow arrows label lipid droplets.

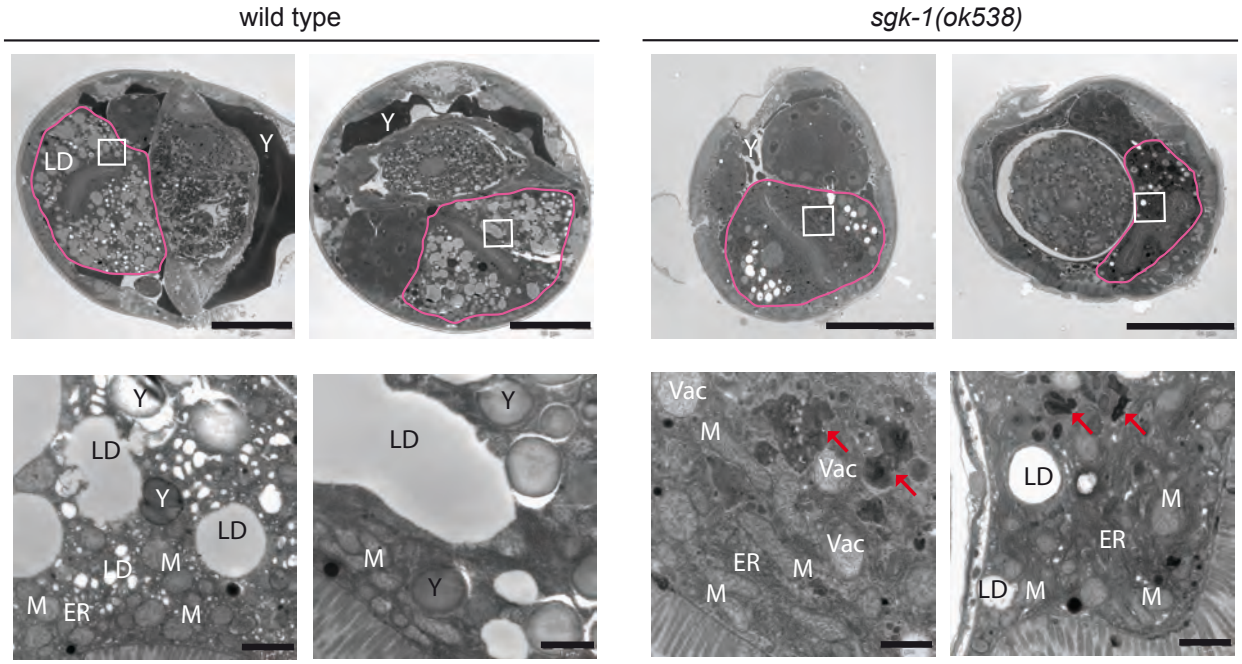

Figure S9: Electron microscopy images of the first intestinal cells of two wild-type and two *sgk-1(ok538)* adults, grown in OP50 bacteria, at day 5 of adulthood. Top images show a general view of a section where the intestine is delineated with a pink line. *sgk-1* mutants show drastically reduced Yolk (Y) and lipid droplet (LD) accumulation in the intestine, as well as reduce lipid content in the hypodermis. Lipoprotein accumulation in the body cavity is also reduced in *sgk-1* mutants compared to wild type worms. White squares are magnified in the bottom images. Bottom images show altered mitochondrial size, reduced LD and Y particles in *sgk-1* mutants. In wild type animals LD emanate from the ER and contribute to both LD and Y formation (left bottom). Such events are not observed in *sgk-1* mutants, instead complex myelinated autophagic structures are observed (red arrows). Bar sizes: 20 µm (top images) and 1 µm (bottom images). M: mitochondria, LD: Lipid Droplets, ER: Endoplasmic Reticulum, Y: Yolk, Vac: Vacuoles.

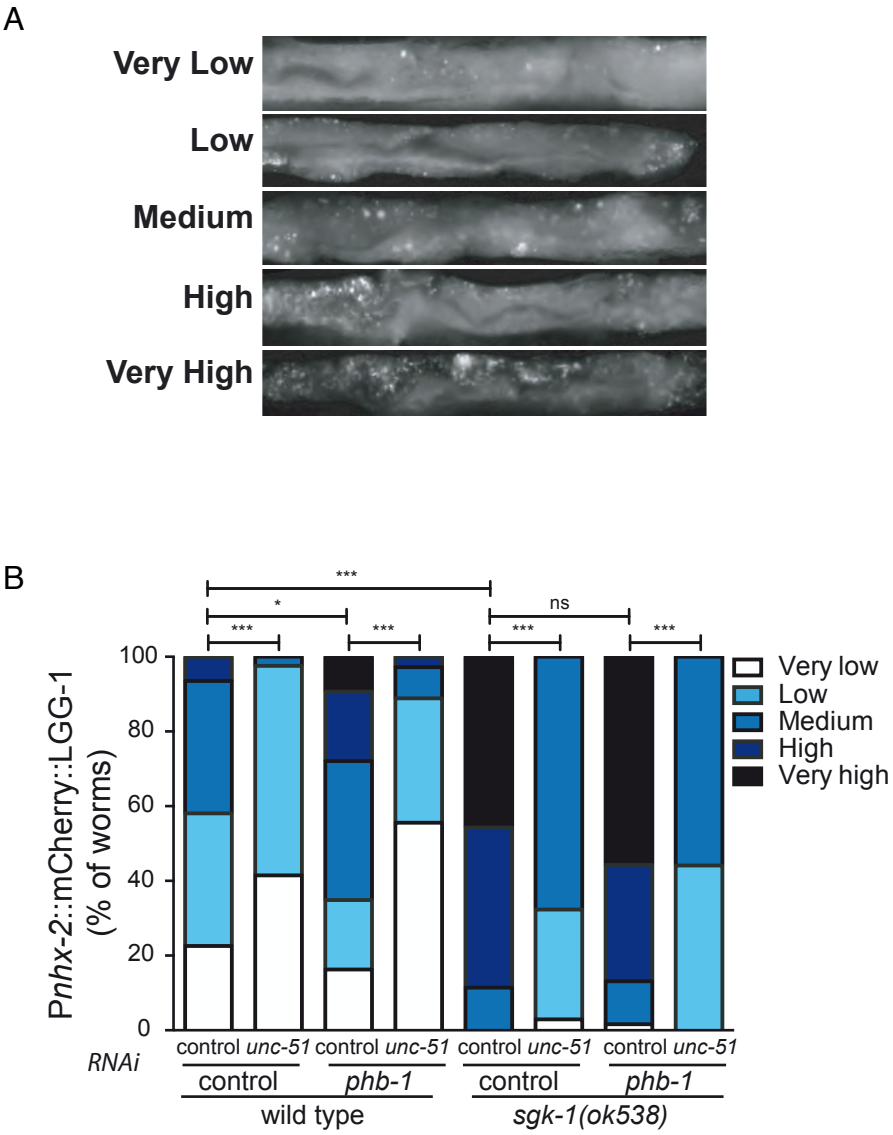

Figure S10: Expression pattern of the autophagy reporter Ex[P*nhx-2*::mCherry::LGG-1]. A. Animals were classified in 5 different categories based on the reporter expression pattern: Very low: animals with a completely diffused expression pattern; Low: animals with a generally diffuse expression pattern but with the presence of small puncta; Medium: animals with puncta along the intestine; High: animals showing aggregation of LGG-1 puncta mostly in the posterior part of the intestine; Very high: animals with large LGG-1 aggregates along the whole intestine. **B.** Quantification of the autophagy reporter Ex[P*nxh-2*::mCherry::LGG-1] in wild type animals, *phb-1(RNAi)* treated worms, *sgk-1(ok538)* mutants and *sgk-1;phb-1 depleted* mutants at day 5 of adulthood under *unc-51(RNAi) treatment.* (*** p value < 0.001, * p value < 0.1, ns not significant; t-test. Combination of at least three independent replicates.).

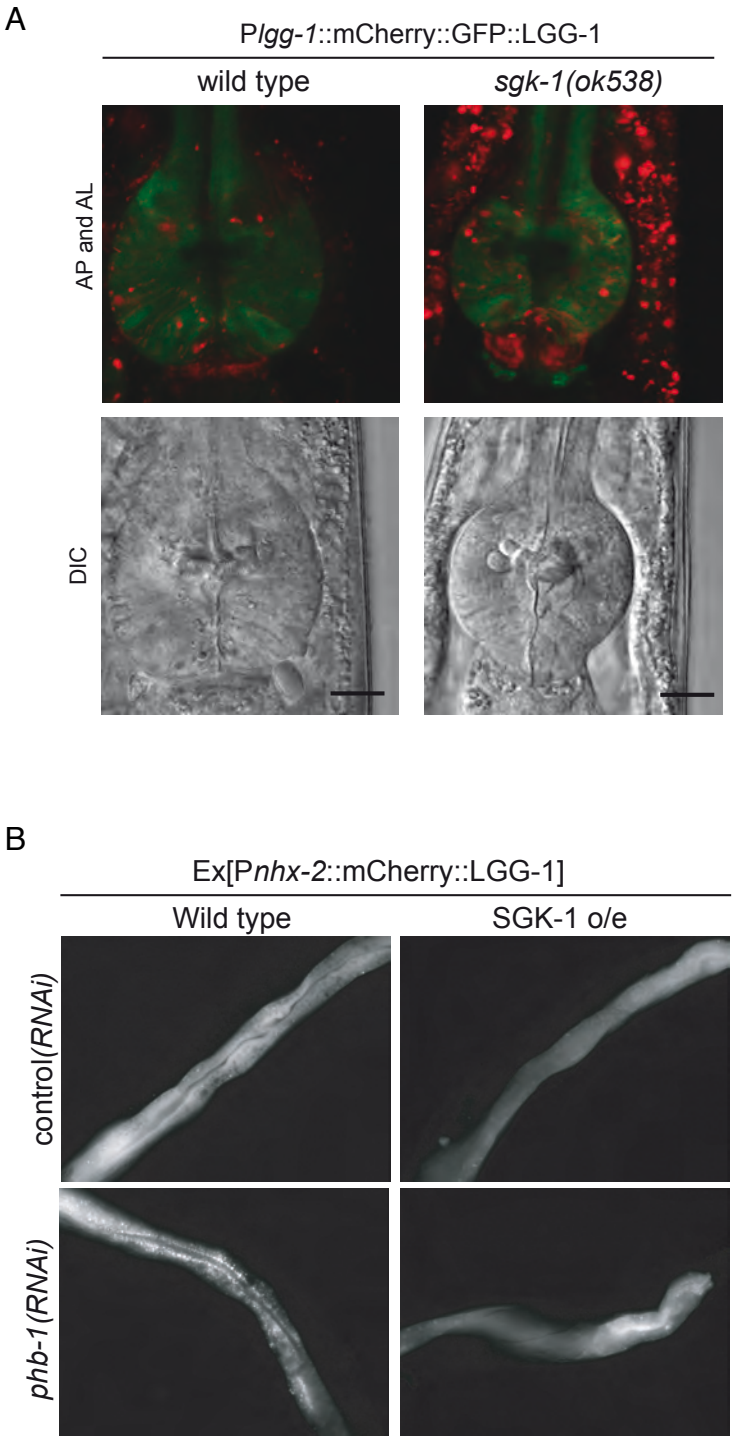

Figure S11: SGK-1 and autophagy. A. Images of the P*lgg-1*::mCherry::GFP::LGG-1 reporter in wild type animals and *sgk-1* mutants at day 5 of adulthood in OP50. Red dots correspond to autophagosomes (AP) and autolysosomes (AL) in the hypodermis and pharynx. Brightfield images are shown in the bottom panel. Bar size: 10 µm. **B.** Ex[P*nhx-2*::LGG1::mCherry] expression pattern in wild type and SGK-1 overexpressing animals, under normal and mitochondrial stress conditions, at day 5 of adulthood. LGG-1 protein shows a completely diffuse expression pattern in worms overexpressing SGK-1 even under mitochondrial stress conditions.

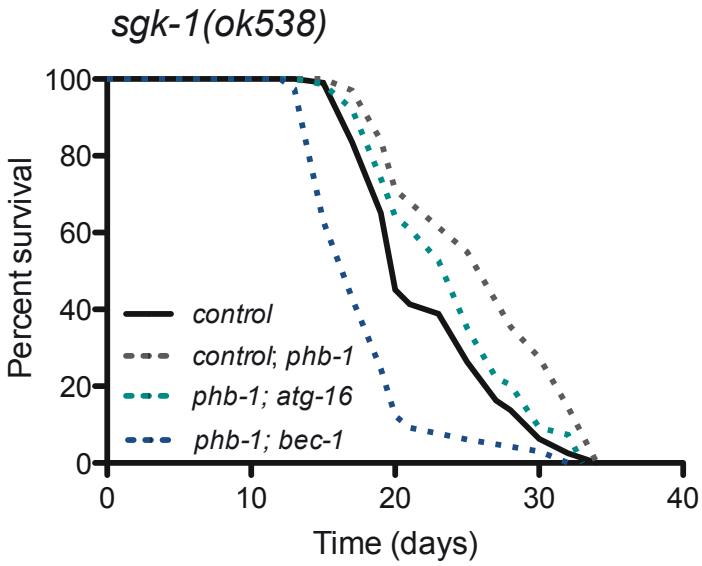

Figure S12: Lifespan assays of *sgk-1* mutants treated with *phb-1(RNAi)* in combination with *atg-16 (RNAi)* and *bec-1 (RNAi).* Replicates and statistics are shown in table S1.

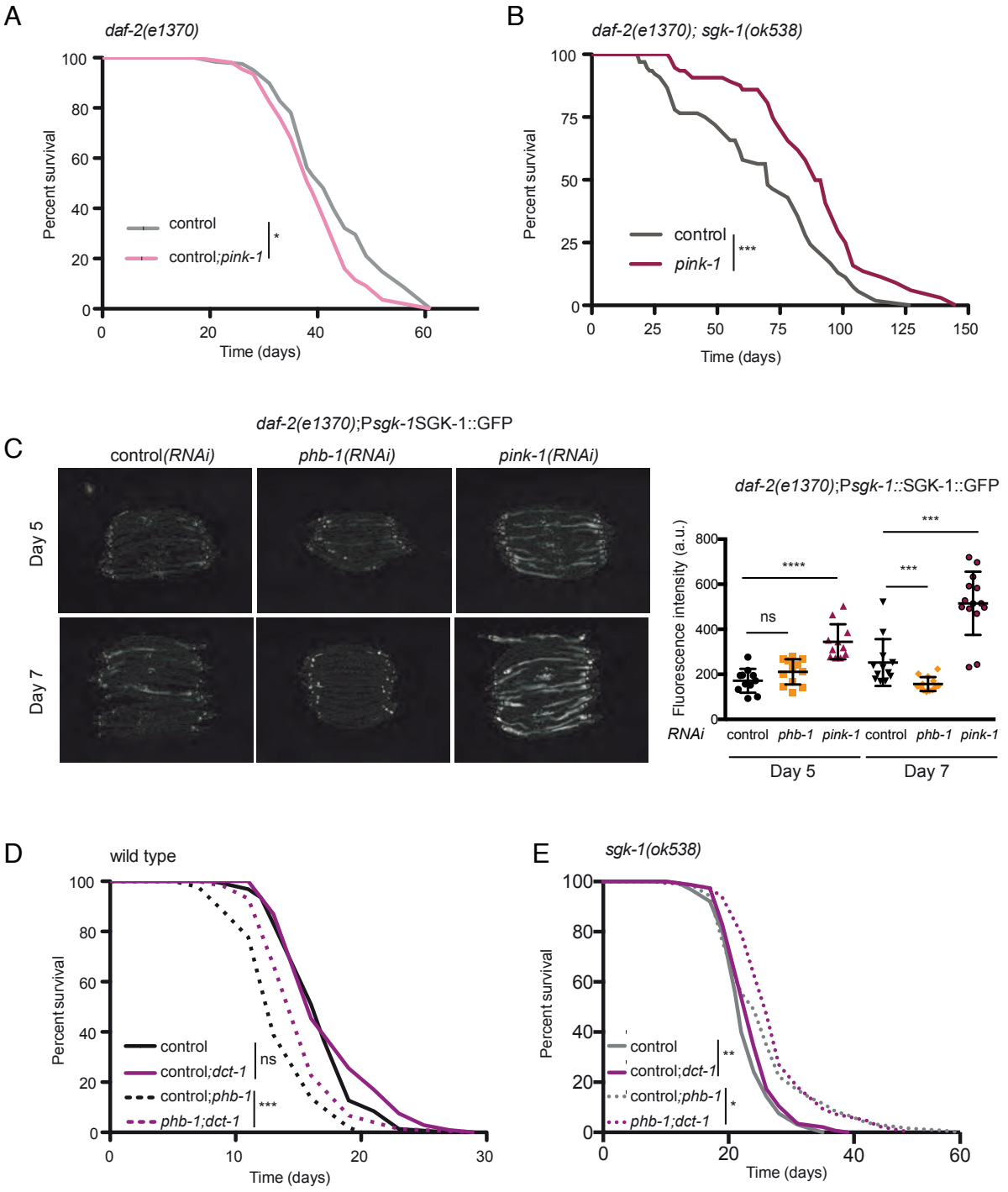

Figure S13: A. Lifespan of *daf-2* mutants treated with *pink-1(RNAi)* diluted with control(RNAi). **B.** Lifespan of *daf-2;sgk-1* double mutants upon inhibition of mitophagy (*pink-1(RNAi)*). **C.** Images of Ex[P*sgk-1*::SGK-1::GFP] expression levels at day 5 and day 7 of adulthood in *daf-2(e1370)* mutants treated with *phb-1(RNAi)* and *pink-1(RNAi)* (right). Quantification of SGK-1 protein levels. (Mean ± SD; *** *p* value < 0.001, ns not significant, t test.). **D.** Lifespan of wild type and *phb-1* depleted worms upon inhibition of mitophagy (*dct-1(RNAi)*). **E.** Lifespan of *sgk-1* mutants and *sgk-1;phb-1(RNAi)* treated mutants upon inhibition of mitophagy (*dct-1(RNAi)*). Lifespan replicates and statistics are shown in table S1.

Table S1: Lifespan data

				P value	
	Median survival	max survival*	# deaths/total	*vs ctrl* RNAi	*vs phb-1* RNAi/NAC-
sgk-1(ok538),ctrl RNAi	20	27	133 / 240		
sgk-1(ok538),ctrl_atfs-1 RNAi	21	26	134 / 240	0,7119 (ns)	
sgk-1(ok538),ctrl_phb-1 RNAi	23	28	143 / 240	0,0013 (**)	
sgk-1(ok538),ctrl_pink-1 RNAi	23	27	122 / 228	0,0020 (**)	
sgk-1(ok538),ctrl_unc-51 RNAi	21	25	95 / 240	0,1403 (ns)	
sgk-1(ok538),phb-1_atfs-1 RNAi	17	22	166 / 240		< 0.0001 (***)
sgk-1(ok538),phb-1_pink-1 RNAi	25	30	157 / 240		0,0008 (***)
sgk-1(ok538),phb-1_unc-51 RNAi	19	24	149 / 240		< 0.0001 (***)
wild type,*ctrl* RNAi	17	21	106 / 160		
wild type,*ctrl_atfs-1* RNAi	18	22	110 / 160	0,3095 (ns)	
wild type,*ctrl_phb-1* RNAi	14	17	62 / 160	< 0.0001 (***)	
wild type,*ctrl_pink-1* RNAi	17	22	115 / 160	0,5091 (ns)	
wild type,*ctrl_unc-51* RNAi	14	17	58 / 160	< 0.0001 (***)	
wild type,*phb-1_atfs-1* RNAi	14	18	107 / 160		0,1535 (ns)
wild type,*phb-1_pink-1* RNAi	16	19	42 / 120		0,0002 (***)
wild type,*phb-1_unc-51* RNAi	13	17	42 / 160		0,9061 (ns)
wild type,*ctrl* RNAi	15	17	54 / 160		
wild type,*ctrl_phb-1* RNAi	14	16	39 / 160	< 0.0001 (***)	
wild type,*ctrl_unc-51* RNAi	14	16	17 / 143	0,0005 (***)	
wild type,*phb-1_unc-51* RNAi	13	14	22 / 138		0,0393 (*)
sgk-1(ok538),ctrl RNAi	23	27	119 / 192		
sgk-1(ok538),ctrl_atfs-1 RNAi	23	26	114 / 200	0,8783 (ns)	
sgk-1(ok538),ctrl_phb-1 RNAi	24	32	131 / 200	0,0002 (***)	
sgk-1(ok538),ctrl_pink-1 RNAi	25	29	75 / 182	0,0025 (**)	
sgk-1(ok538),ctrl_unc-51 RNAi	25	26	110 / 200	0,1484 (ns)	
sgk-1(ok538),phb-1_atfs-1 RNAi	19	23	134 / 199		< 0.0001 (***)
sgk-1(ok538),phb-1_pink-1 RNAi	25	29	113 / 193		0,6703 (ns)
sgk-1(ok538),phb-1_unc-51 RNAi	20	23	108 / 173		< 0.0001 (***)
wild type,*ctrl* RNAi	17	21	75 / 115		
wild type,*ctrl_dct-1* RNAi	16	23	107 / 125	0,1355 (ns)	
wild type,*ctrl_phb-1* RNAi	13	17	56 / 102	< 0.0001 (***)	
wild type,*ctrl_pink-1* RNAi	16	21	103 / 125	0.5787 (ns)	
wild type,*phb-1_dct-1* RNAi	16	19	80 / 123		0,0004 (***)
wild type,*phb-1_pink-1* RNAi	16	21	73 / 116		< 0.0001 (***)
sgk-1(ok538),ctrl RNAi	21	26	113 / 150		
sgk-1(ok538),ctrl_dct-1 RNAi	22	38	134 / 150	0,0224 (*)	
sgk-1(ok538),ctrl_phb-1 RNAi	28	40	117 / 150	< 0.0001 (***)	
sgk-1(ok538),ctrl_pink-1 RNAi	24	28	126 / 150	0,0091 (**)	
sgk-1(ok538),phb-1_dct-1 RNAi	26	38	98 / 150		0,0097 (**)
sgk-1(ok538),phb-1_pink-1 RNAi	31	27	93 / 150		0,7601 (ns)

sgk-1(ok538),ctrl RNAi_NAC-	17	24	131 / 150		
sgk-1(ok538),ctrl RNAi_NAC+	19	24	127 / 150		0,0097 (**)
sgk-1(ok538),ctrl_phb-1 RNAi_NAC-	24	35	112 /150	< 0.0001 (***)	
sgk-1(ok538),ctrl_phb-1 RNAi_NAC+	21	28	115 / 150		< 0.0001 (***)
sgk-1(ok538),ctrl RNAi_NAC-	19	26	112 / 126		
sgk-1(ok538),ctrl RNAi_NAC+	20	24	102 / 126		0,9379 (ns)
sgk-1(ok538),ctrl_phb-1 RNAi_NAC-	21	31	105 / 126	0.0001 (***)	
sgk-1(ok538),ctrl_phb-1 RNAi_NAC+	20	26	107 / 126		0,0003 (***)
wild type,*ctrl* RNAi_NAC-	18	21	86 / 126		
wild type,*ctrl* RNAi_NAC+	17	20	79 / 126		0,2159 (ns)
wild type,*ctrl_phb-1* RNAi_NAC-	16	19	85 / 126	< 0.0001 (***)	
wild type,*ctrl_phb-1* RNAi_NAC+	14	17	66 / 126		0,0004 (***)
daf-2(e1370),ctrl RNAi	41	56	95 / 150		
daf-2(e1370),ctrl_pink-1 RNAi	39	49	82 / 150	0,0112 (*)	
sgk-1(ok538),ctrl RNAi	19	25	147 / 150		
sgk-1(ok538),ctrl_dct-1 RNAi	22	27	132 / 150	< 0.0001 (***)	
sgk-1(ok538),ctrl RNAi	22	28	136 / 168		
sgk-1(ok538),ctrl_dct-1 RNAi	24	31	146 / 167	0,0071 (**)	
sgk-1(ok538),phb-1_dct-1 RNAi	26	35	139 / 169		0,0477 (*)
sgk-1(ok538), ctrl RNAi	32	39	127 / 180		
sgk-1(ok538);sod-1(tm776)	27	32	142 / 180	< 0.0001 (***)	
sgk-1(ok538);sod-2(gk257)	32	41	141 / 180	0,0002 (***)	
wild type,*ctrl* RNAi	19	28	147 / 180		
sod-1(tm776)	19	28	154 / 180	0,1214 (ns)	
sod-2(gk257)	25	34	164 / 180	< 0.0001 (***)	
sgk-1(ok538), ctrl RNAi	29	36	104 / 180		
sgk-1(ok538);sod-1(tm776)	27	34	123 / 180	0,0106 (*)	
sgk-1(ok538);sod-2(gk257)	32	41	110 / 180	0,0093 (**)	
wild type,*ctrl* RNAi	19	28	140 / 180		
sod-1(tm776)	21	28	155 / 180	0,3612 (ns)	
sod-2(gk257)	22	32	155 / 180	< 0.0001 (***)	
wild type,*ctrl* RNAi	20	25	147 / 180		
wild type,*ctrl_atfs-1* RNAi	20	25	145 / 180	0,3861 (ns)	
wild type,*ctrl_phb-1* RNAi	18	22	124 / 180	0,0001 (***)	
wild type,*phb-1_atfs-1* RNAi	18	22	152 / 180		0,7498 (ns)
d*af-2(e1370);sgk-1(ok538),ctrl* RNAi	70	104	62 / 151		
daf-2(e1370);sgk-1(ok538),pink1 RNA	89	121	50 / 144	< 0.0001 (***)	
sgk-1(ok538),ctrl RNAi	20	30	82 / 308		

sgk-1(ok538),ctrl_phb-1 RNAi	27	34	62 / 289	< 0.0001 (***)	
sgk-1(ok538),ctrl_pink-1 RNAi	25	30	71 / 241	0,0413 (*)	
sgk-1(ok538),phb-1_atg-16 RNAi	25	30	58 / 280		0,0036 (**)
sgk-1(ok538),phb-1_bec-1 RNAi	17	21	34 / 133		< 0.0001 (***)
sgk-1(ok538),phb-1_pink-1 RNAi	27	34	87 / 257		0,6784 (ns)
wild type,*ctrl* RNAi_NAC-	19	27	85 / 149		
wild type,*ctrl* RNAi_NAC+	15	23	51 / 104		0,0001 (***)
wild type,*ctrl_phb-1* RNAi_NAC-	19	27	66 / 149	0,019 (*)	
wild type,*ctrl_phb-1* RNAi_NAC+	15	27	82 / 141		0,0005 (***)

P values were calculated using the log-rank test, as described in Methods.

* day where more than 90% of population is dead

#The number of confirmed death events, divided by the total number of animals included the assays is sh

Total equals the number of animals that died plus the number of animals that were censored.

Total equals the number of animals that died plus the number of animals that